2015

# Frequency-Domain Faraday Rotation Spectroscopy (FD-FRS) for Functionalized Particle and Biomolecule Characterization

Richard Murdock
*University of Central Florida*

# FREQUENCY-DOMAIN FARADAY ROTATION SPECTROSCOPY (FD-FRS) FOR FUNCTIONALIZED PARTICLE AND BIOMOLECULE CHARACTERIZATION

by

RICHARD JOSHUA MURDOCK

A thesis submitted in partial fulfillment of the requirements
for the Honors in the Major Program in Mechanical Engineering
in the College of Engineering and Computer Science
and in the Burnett Honors College
at the University of Central Florida
Orlando, Florida

Spring Term 2015

Thesis Chair: Shawn A. Putnam, Ph.D.

# ABSTRACT

In this study, the magnetically-induced vibrations of functionalized magnetic particle suspensions were probed for the development of a novel optical spectroscopy technique. Through this work (1) the frequency-dependence of the faraday rotation in ferrofluids and (2) the extension of this system to elucidating particle size and conformation as an alternative immunoassay to costly and labor/time intensive Western Blotting and ELISA has been shown. With its sensitivity and specificity, this method has proven to be a promising multi-functional tool in biosensing, diagnostic, and therapeutic nanomedicine efforts. Due to its ubiquitous nature in all optically-transparent materials, the faraday rotation, or circular birefringence, was developed as a robust and sensitive nanoscale biomolecule characterization technique through Brownian relaxation studies of particle suspensions. Current efforts have shown the applicability of this phenomenon in solid, pure liquid, and colloidal samples as well as simultaneous advancements of magnetic nanoparticle research in the magnetometric and magneto-optical regimes. By merging these two fields, a clinically relevant spectroscopy (fd-FRS, Frequency Domain Faraday Rotation Spectroscopy) was developed based on a newly revised model stemming from Debye relaxation theory. Through this work, an optical bench with a variable permeability core electromagnet and a frequency-domain lock-in amplifier setup (DC to 20 kHz) have been used to distinguish between $Fe_3O_4$-core nanoparticles with functionalization layers of PEG4/PEG8 polymer with future applications involving the Anti-BSA/BSA antibody/antigen couple. Particle concentrations down to 500 nM (magnetic nanoparticles) and 0.01 Volume % (magnetic beads) were studied with diameters ranging from 200 nm to 1 $\mu$m. Currently, the characteristic peak corresponding to the out-of-phase relaxation of the suspended particles has been elusive, despite a wide particle size distribution and the use of a balanced photodetector. Future work will involve highly monodisperse samples, faster scan times, and thermal characterization applications of fd-FRS.

# DEDICATION

For my family and friends
through all and in all,
you have been my inspiration and my strength.

# ACKNOWLEDGMENTS

There are not words to fully voice my appreciation for the mentorship, support, guidance, knowledge, and patience of my adviser, Dr. Shawn Putnam. From the planting of the seed of an idea that blossomed into one of my most rewarding educational and career-shaping experiences of my life, Dr. Putnam has nurtured my scientific curiosity, spend countless hours training me, working with me, and showing me that diligence makes for the most meaningful discoveries. This is to his vision and his constant belief in me, even through all the diffcult times. I would also like to thank my thesis committee members Dr. Yongho Sohn and Dr. Hansen Mansy, for their time and support. Without their honest opinions and recommendations, this thesis would not be where it is today.

I would also like to thank my collaborators, Dr. Sudipta Seal, Dr. Soumen Das, and Ankur Gupta from the UCF Materials Characterization Facility (MCF) and the Advanced Materials Processing and Analysis Center (AMPAC) for the supply of constructive criticism and unique perspectives, a source of inspiration, and a voice of constancy. The materials they have provided have been the bedrock on which the results presented here are laid.

I also wish Kevin Gleason, Alan Nehemy, Adam Phillips, Elyse Chase, and Alex Chavez the best of luck in all future endeavors. As my labmates over the years, they have both supported and driven me, giving me more than a few laughs and the opportunity to leave a meaningful legacy. In their future plans toward academia, industry, or other scientific endeavors, I wish them the best of luck and hope to have the pleasure of working along side them once again one day.

I extend my thanks to the Burnett Honors College, Department of Mechanical and Aerospace Engineering, and the Office of Undergraduate Research for the opportunities, support, and guidance they provided me. This research would not have been possible without them.

# TABLE OF CONTENTS

# LIST OF FIGURES

# LIST OF TABLES

# NOMENCLATURE

| | |
|---|---|
| $A$ | Area |
| $B$ | Magnetic Field Strength (B-field) |
| $B(\omega)^{real}$ | Real Component of the Measured Magnetic Field Strength |
| $B(\omega)^{imag}$ | Imaginary Component of the Measured Magnetic Field Strength |
| $C$ | Degrees Celsius |
| $C_{V\%}$ | Suspension Concentration in Volume Percent |
| $C_{mol}$ | Colloid/Suspension Concentration in Molar Concentration |
| $D_h$ | Hydrodynamic Diameter |
| $E_a$ | Thermal Activation Energy Barrier |
| $f$ | Frequency |
| $H$ | External Magnetizing Field |
| $i$ | Imaginary Number, $\sqrt{-1}$ |
| $I$ | Laser Intensity |
| $K$ | Kelvin |
| $k_b$ | Bolzmann Constant |
| $l$ | Optical Pathlength |
| $LABVIEW$ | Measurement Software |
| $m$ | Magnetization |
| $Mathcad$ | Computation and Graphing Software Interface |
| $M_w$ | Molecular Weight |
| $n$ | Index of Refraction |
| $t$ | Time |
| $T$ | Temperature |
| $V$ | Voltage |

| | |
|---|---|
| $V(\omega)^{real}$ | Real Component of the Measured Lock-In Amplifier Voltage |
| $V(\omega)^{imag}$ | Imaginary Component of the Measured Lock-In Amplifier Voltage |
| $V_h$ | Hydrodynamic Volume |
| $XGen$ | Computation and Graphing Software Interface |
| $Z$ | Zeta Potential |

## Greek

| | |
|---|---|
| $\alpha$ | Offset Angle from Minimum on Photodiode Response Curve |
| $\beta$ | Offset Angle on Polarizer |
| $\epsilon_0$ | Vacuum Permittivity |
| $\eta$ | Dynamic Viscosity |
| $\theta$ | Faraday Rotation Angle |
| $\theta(\omega)^{real}$ | Real Component of the Faraday Rotation |
| $\theta(\omega)^{imag}$ | Imaginary Component of the Faraday Rotation |
| $\lambda$ | Wavelength |
| $\mu$ | Relative Magnetic Permeability |
| $\mu_o$ | Magnetic Permeability of Free Space |
| $\nu$ | Verdet Constant |
| $\nu(\omega)^{real}$ | Real Component of the Verdet Constant |
| $\nu(\omega)^{imag}$ | Imaginary Component of the Verdet Constant |
| $\rho$ | Density |
| $\tau_B$ | Brownian Relaxation Time Constant |
| $\tau_N$ | Neel Relaxation Time Constant |
| $\phi$ | Phase Lag of Magnetic Field |
| $\omega$ | AC Circular Frequency |

## Acronyms

| | |
|---|---|
| Anti-BSA | Anti-Bovine Serum Albumin Antibody Complex |
| BSA | Bovine Serum Albumin |
| DAQ | Data Acquisition Board |
| PDMS | Polydimethylsiloxane |
| MNP | Magnetic Nanoparticle |
| MNP.PEG4 | MNP Core with Layer 1 (PEG4) |
| MNP.PEG8 | MNP Core with Layer 2 (PEG8) |
| MNP.PEG4.Anti-BSA | MNP Core Layer 1 (PEG4), Layer 2 (Anti-BSA) |
| MNP.PEG4.Anti-BSA.BSA | MNP Core Layer 1 (PEG4), Layer 2 (Anti-BSA), Layer 3 (BSA) |
| PEG | Polyethylene Glycol |
| PEG4 | Polyethylene Glycol, Low Molecular Weight |
| PEG8 | Polyethylene Glycol, High Molecular Weight |

# CHAPTER 1: INTRODUCTION

## 1.1 Background

### 1.1.1 Magneto-Optical Phenomenon

For centuries, man has recorded his fascination in the interaction of light with matter. From the construction of the first projector and lens to the development of laser and the discovery of the polarizations of light, science has been advancing at a truly outstanding pace in understanding the ubiquitous yet explicatively-elusive phenomenon called electromagnetic radiation. In particular, the coupling of magnetism and electric fields as well as the interaction of light with these two, has formed the basis of much research in recent years. In particular, three such useful phenomena have emergedfor the study of molecular, nano-scale, and micro-scale materials and their interactions with their environment: Faraday Rotaton, Kerr Rotation, and Dichroism. Birefringence, the difference in propagation speed of electromagnetic radiation of different polarizations as it travels in or reflects from a material, forms the basis for the first two effects. Faraday Rotation takes into account the changes in such waveforms during the transmission of light through a transparent or semi-transparent medium with a net magnetization inthe direction of light propagation. Kerr Rotation behaves in a similar manner with the exception of the reflection of light rather than its transmission being of critical importance. Dichroism is a natural difference in the absportivity of a medium for different polarizations of light, related to but not exactly falling under the same category as the previous two "effects." It should be noted that any material that exhibits birefringence will to some extent also exhibit dichroism, and most measured responses are a superposition of the two. It is then the purpose of this work to further the understanding of the ability of scale-specific scientific knowledge and engineering manipula-

tion to probe the dynamics, interactions, and behavior at the molecular, nano, and micro scales to thus increase sensitivity of characterization measurements beyond current levels. It is expected that this work will help form the base for an economical approach to single molecule analysis from a new perspective using the Faraday Rotation magneto-optical effect and magnetic particles at varying length scales.

### 1.1.2 Magnetic Nanoparticles: Properties and Underlying Phenomena

One of the many benefits of nano and micro-scale research is the very dimension in which it operates. In most classical applications, the term nanoparticle is restricted to materials with dimensions on the order of 1 to 100 nm. Typically, materials and composites larger than this through the $\mu$m range, but still small enough to be subject to unique quantum and magnetic domain principles (not more than a few micrometers), are called beads. There are a many types of particles usually classified by their overall dimensions and composition. To benefit a specific and well-developed area of nanoparticle research, the focus of this study will be on magnetic iron oxide nanoparticles and beads, especially those in colloidal or suspended form, called ferrofluids. For simplicity in description, and to more broadly and accurately cover the range of sizes available and studied, both nanoparticles and beads will be referred to as particles in this work.

A fundamental governing principle in the study of magnetic materials is the concept of relaxation. Due to magnetic moment alignment within materials under the influence of an external field (H), a net magnetization is developed. This process, however, takes a certain amount of time to complete. Similarly, the removal of the H field is also accompanied by a transition from an organized or semi-organized magnetized state to a thermodynamically equilibrated one corresponding to either a remanent magnetization in the direction of the "easy" or fast axis, or a randomly oriented one due to entropic randomization of the magnetic moments. The energy barrier to an internal reorientation is known as the anisotropy energy

[32]. Overcoming this barrier is accomplished according to the Néel relaxation mechanism. The thermal dependence of this process is expressed by the Néel relaxation time constant

$$\tau_N = \tau_0 exp(\frac{E_B}{k_B T}) \tag{1.1}$$

where $\tau_0$ is a temperature and field dependent parameter called the attempt time, $E_B$ is the anisotropy energy barrier equal to $KV(1 - \frac{H}{H_{sw}})$ where $\frac{H}{H_{sw}}$ is the ratio of the applied field to the anisotropy field in the case of aligned particles and KV is the product of the particle anisotropy constant and its volume[14], $k_B$ is the Boltzmann constant, and $T$ is the system temperature. Interestingly, the size-dependence of the domain formation in magnetic materials reaches a limit where it is no longer favorable to split the material into several domains of uniform magnetic moment. Instead, a single domain structure is formed which has only one magnetization or magnetic moment. When the anisotropy barrier of a single domain structure is lower than the thermal energy fluctuations (as is usually the case for room temperature nanoparticles) the ensemble is considered to have entered the superparamagnetic realm [14, 32]. Characteristic of this region is the lack of remanence and a consequent lack of hysteresis. There is still a time associated with the loss of remanence, but it is very short compared to the experimental time frame [14]. This phenomenon is especially useful when studying the miniturization of domain formation and its time dependence as well as the thermodynamics of nanoscale magnetization, as seen in the three cases presented in Fig. 1.1. The three energy barriers encountered between opposing moments can be seen to vary according to the applied field direction and the existence of a single domain structure. Critical size ranges for the transition into the superparamagnetic state varies by material, and these values are tabulated by Thanh et al. [32].

A second relaxtion method characteristic of mobile magnetic elements is Brownian re-

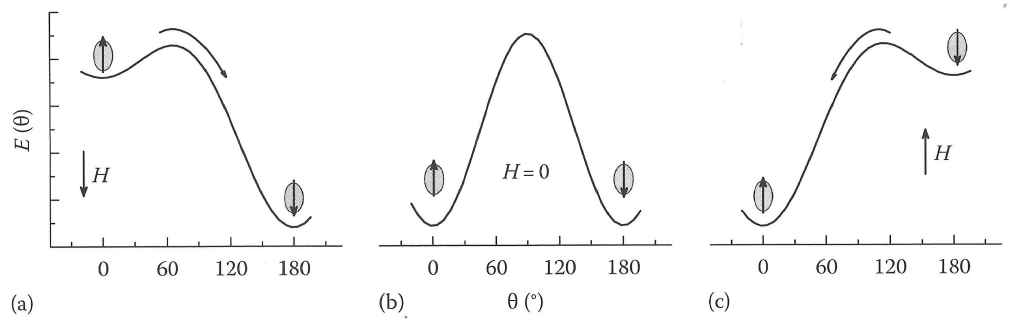


**Figure 1.1:** Single domain structure overcoming the aniotropy barrier a) with external field, b) with no field and c) against the external field [32]

laxation expressed by a Brownian relaxation time

$$\tau_B = \frac{6V_h\eta}{k_BT} \tag{1.2}$$

where $V_b$ is the hydrodynamic radius of the particle, $\eta$ is the dynamic viscosity of the solvent in which the particles are suspended, $k_b$ is the Boltzmann constant, and $T$ is the temperature of the system, in Kelvin. In this mechanism, whole particles rotate or realign due to their interactions with their environment, usually a solvent [14]. Although this mechanism does contribute to overall relaxation times, for a given measurement time scale, its effect is detectable at a different size distribution compared to that covered by the Néel mechanism and varies according to solvent properties. In the case of colloidal suspensions, larger particles, more viscous solvents, and lower temperatures cause the particle to rotate more slowly, meaning a longer net magnetization and a slower response. This concept has been explored by researchers in the field seeking to understand aggregation and solid phase relaxation inhibition of agglomerated nanoparticles with protein coatings [20, 21, 23]. A comparison of one such system of ferric oxide particles was used to probe the time scales associated with each of these relaxation processes and the domains over which they operate as seen in Fig.

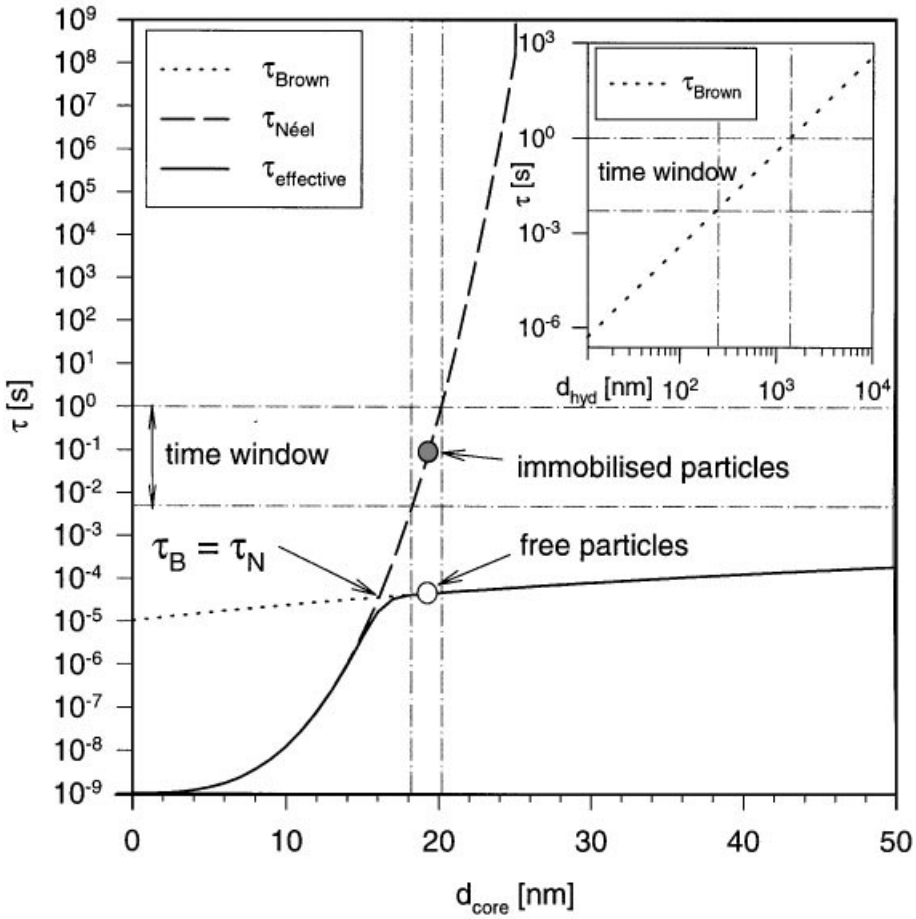


**Figure 1.2:** Comparison of example demagnitization time scales (Brownian vs. Neel) for colloidal particles as a function of core diameter. [20]

1.2 [20]. From this figure, it is derived that at the smallest sizes of particles, Néel relaxation forms the major contribution to magnetic relaxation (fastest response) as the particle relaxes internally by overcoming an overall smaller energy barrier before the particle has time to physically rotate. Brownian relaxation takes precendence after a core size of approximately 12 to 15 nm as the core magnetization must overcome a larger energy barrier and thus the thermal agitations and randomizations take a more important role.

Two other important features of magnetic particle studies are surface modification or functionalization and external manipulation [32]. Either to protect them from external

corrosion or degredation, give them functional surface components, or stabilize them under differing environmental conditions, surface functionalization and coatings provide a way to play on the large surface area to volume ratio characteristic of particles. Both simple and complex molecules have been attached to change the zeta potential, hydrophobicity, or even the magnetization of particles [32]. External manipulation is arguably one of the most popular applications of the strong magnetic behavior of magnetic particles. Specifically, these can be directed from a distance and controlled to form various shape, assume any profile, or separate from an otherwise complex arrangement of materials by the application of an external aligning field.

# CHAPTER 2: LITERARY REVIEW

The characterization of compounds via interaction with magnetic particles has taken many shapes and forms in the literature. The attractiveness of the use of particles is their multifunctionality and unique properties [10, 32]. In particular, two major subclasses of measurement systems have taken precendence in recent research: 1) magneto-optical interactions and 2) magnetic remanence and resonance. These two groups encompass the applicability of magnetic nanoparticles in a variety of settings, as mentioned earlier, depending on the need to separate the measurement device from the sample to reduce noise and intereference or bring nanoparticle characterization into the biological scene as such material exhibits only weak magnetism, thus allowing for great contrast.

## 2.1 Faraday Rotation: Past and Present

As mentioned in the introduction, among other magneto-optic interactions, the faraday rotation (circular birefringence) is both well-known and well-studied in optics research today. Faraday rotation occurs when a plane-polarized light beam propagates through a magnetized material. One polarization is retarded relative to the other through a material anisotropy and the overall waveform recombines at a slightly different polarization angle (having acquired a net rotation). The familiar underlying physical equation for this phenomena is given by [38]

$$\theta = B\nu l \tag{2.1}$$

where $\theta$ is the angle of rotation of the polarized waveform, $\nu$ is the verdet constant of the material (a material property), B is the magnetic flux density, and l is the path length of the interacting beam and magnetized material. The verdet constant is of particular interest

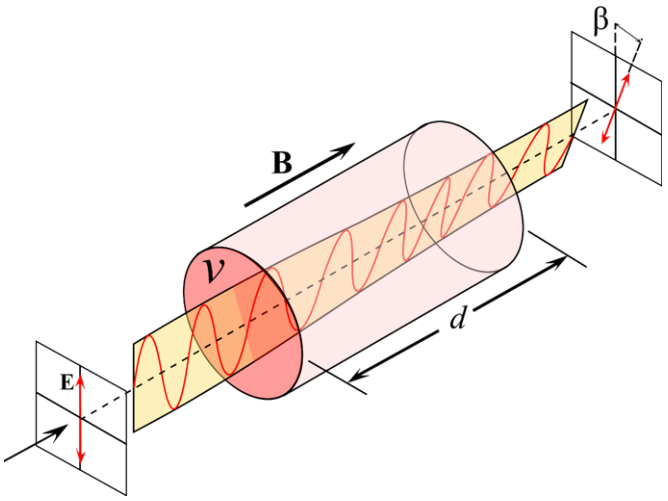


**Figure 2.1:** Faraday Rotation example in generc medium. The notation of the parameters in this figure are slightly different compared to the expression in Eq. 2.1 (d is the pathlength and $\beta$ is the faraday rotation angle). Photo courtesy of *en.wikipedia.org/wiki/*

because it describes the only material property in the equation and controls the extent to which any material rotates plane polarized light under identical magnetic field and pathlength conditions. This phenomenon can be visualized by the graphic in Fig. 2.1.

Interestingly, despite their apparent similarities, faraday rotation differs from circular dichroism in that it does not require chiral molecular arrangements or unique strutures with different absorptivities of light polarizations to produce optical anisotropy [26]. Instead, all transparent materials exhibit faraday rotation to a particular extent, as determined by their verdet constant. Thus, characterization techniques based on faraday rotation are robost in nature for materials characterization. For example, the true usefulness of faraday rotation can be seen by passing the rotated waveform through an analyzer, thus converting a polarization change into a light intensity change [38]. This result is governed by Malus' law for a simple polarizer/analyzer system

$$I = I_o \cos^2(\beta + \theta) \tag{2.2}$$

where $I_o$ is the maximum intensity of light before the sample, $\beta$ is the relative angle between the initial polarizer and the analyzer, and $\theta$ is the faraday rotation angle. Thus, monochromatic light can be used for nearly any material to determine at least one material property.

One of the greatest advantages of magneto-optical farday rotation measurement is the separation of the measurement instruments and the system under study. This prevents interference between the sensitive samples being probed and the geometric arrangement of the experimental set up. The main advantage is reduced noise and increased versatility in arranging system components and modifying detection techniques. Compared to magnetometry techniques such as those utilized by a Superconducting Quantum Interference Device (SQUID), the samples are quite isolated. The only major external disturbance of the system is the interaction of the plane polarized laser with the sample.

With the faraday effect well known for many years, Villaverde et al. [36] characterized 11 liquids of interest reporting their verdet constants as comparison parameters. Using a pulsed magnetic field duration of 10 ms and maximum field intensity of 35 kG, they were able to investigate and compare the magneto-optical response of pure diamagnetic materials. Due to the frequency dependence of the faraday effect, a full characterization involved a range of wavelengths from 347.1 nm to 694.3 nm, spanning a great portion of the visible spectrum (approximately 400 to 800 nm) with a maximum error of approximately $\pm 4\%$. Of particular interest to biologically relevant research were the results for pure water. In this case, a positively concave, monotonically decreasing polynomial curve fit was used to describe the behavior of the system. Interestingly, Villaverde et al. [36] reported a discrepancy of previous research in the field due to the hysteresis effect of the Faraday Rotation effect under the influence of rapidly oscillating magnetic fields, defined by a semiperiod of 58 $\mu$s (a frequency of approximately 8.6 kHz). This will prove to be of interest in the current study as fields ranging from DC to several kHz will be considered.

Wang et al. reported results for faraday rotation observed in ferrofluid [38]. Using both switched DC and low frequency AC fields, they were able to show a difference between the interaction of a polarized beam with a solid phase magneto-optical material and that with a ferrofluid. The well-established theory of the non-reciprocity of faraday rotation in magneto-optic solids was adapted to include nanoparticle-sized materials. This theory essentially stated that the rotation of light propagating through a material reverses with both a reversal of the field and a reversal of the direction of the beam[26, 38]. Thus, when multiple passes through a solid sample are produced, a cumulative, additive rotation angle is achieved. However, when studying 8 nm magnetite particles suspended in water, placed in a 6 $\mu$m fluid cell, and probed with a 650 nm wavelength, 5 mW laser, they observed a symmetric faraday rotation signal, indicating rotation in the same direction regardless of the direction of the applied field. They concluded that at low frequencies the particles rotate under the influence of Brownian motion to align their magnetic moments with that of the applied field, thus effectively demonstrating a reciprocity of the faraday rotation. The key consideration here was that the particles had enough time to relax according to Brownian relaxation due to a slowly varying field of approximately 30 Hz. Higher frequency field oscillations could likely exhibit a transient response or hysteresis effect of the faraday rotation [36]. Thus, solid phase magneto-optical effects may not apply to ferrofluid colloidal suspensions when frequency dependence becomes key, at particular particle sizes. Specifically, at low AC frequencies, the particles would have enough time to follow the switching field, showing overall reciprocity in faraday rotation. After a certain frequency, the magnetic field swtitches faster than the particles can react by Brownian rotation, effectively preventing or diminishing motion. At these higher frequencies, in particles of a size where the contribution of Néel relaxation is negligible for the measurement time of interest, the non-reciprocity of faraday rotation will likely appear as it does in solid phase experiments.

In an effort to a further improve the sensitivity and applicability of faraday rotation to

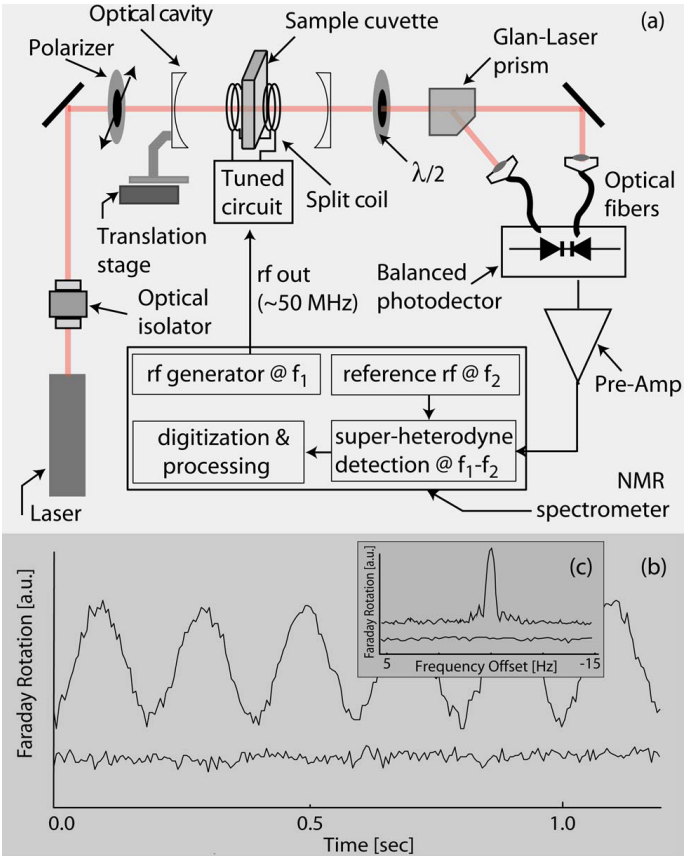


**Figure 2.2:** Experimental setup for cavity-enhanced faraday rotation studies [26]

material characterization, Pagliero et al. studied a novel, optical cavity-enhanced faraday rotation in their development of Optically-Detected Nuclear Magnetic Resonance (ODNMR) [26]. Subjecting fluid samples to radio frequency (rf) oscillating magnetic fields, they were able to apply a commercial NMR spectrometer to study magnetic resonance imaging and spectroscopy, as shown in Fig. 2.2. In an attempt to increase the sensitivity of systems compared to single pass faraday rotation techniques [36, 38], a high finesse optical Fabry-Perot cavity [15, 26] was developed to increase the number of passes through the sample for cumulative faraday rotation [26, 38]. The sample magnetization was driven at 50 MHz with a 10 turn split coil operating near 0.2 mT and a $\lambda$=632 nm, 20 mW laser was used to probe the interaction in a 3 mm water-filled cuvette. By controlling the offset between

the demodulating frequency and the driving frequency, a beating phenomenon was observed that yielded the magnitude of the faraday rotation upon FFT analysis. The reported signal amplification was shown to be 20x greater than that obtained from a single pass. With this result also came a relatively meager 1.5-fold increase in the sensitivity due to a variety of factors. For comparisom, these results were $\sim$3x10$^{-7}$ rad$/\sqrt{Hz}$ for the multiple passes and $\sim$2x10$^{-7}$ rad$/\sqrt{Hz}$ for a single pass. One of the main results was that, with full laser intensity, the single pass measurements yielded a better absolute signal-to-noise ratio than the cavity-enhanced measurements. This was significant since the absorption losses, Rayleigh and sample inhomogeneity scattering, as well as the reflection at the various interfaces between materials of different indices of refraction introduced noise into the system [26]. As seen in Fig. 2.2, a gradual drift or "walk off" the optical axis was also reported, which was caused by the disparity between the curved wavefront of the optical cavity mirrors and the planar faces of the cuvette. Despite these limitations, the versatility of the commerical spectrometer to analyze and process faraday rotation signals, the ability to fine-tune the laser to probe a large class of materials, and the obvious amplification of signal amplitude for use in studying small or barely-varying changes in magneto-optical materials makes this method an attractive and promising technique for future nanoscale faraday rotation measurements.

## 2.2 Optical Spectroscopy

Of particular interest to the field of molecular characterization is optical spectroscopy. In its most rudimentary form, optical spectroscopy can be defined as the study of the interaction between electromagnetic radiation and a material [18, 33]. The majority of spectroscopic methods involve the absorption, transmission, emission, reflection, or scattering of light. These interactions are usually governed by vibratory responses (stretching or bending of bonds), the index of refraction of materials, and crystallographic properties. For instance,

IR spectrometers (typically FT-IR) probe the transmission of IR light as it passes through a sample since certain bonds absorb photons of just the right energy to temporarily excite them, thus revealing the bond character of the material [18]. More macroscopically in the realm of the electromagnetic spectrum, the electronic, vibrational, and rotational motion of molecules can be probed with correspondingly increasing wavelengths depending on the specific energy level they require for excitation [33]. In the case of IR spectroscopy, the far IR range revealed the absorbances of the bonds of interest. Another example is UV-Vis spectroscopy, which gives clues as to the extent of conjugation present in molecules mostly in the visible range.

NMR spectroscopy [18] is more closely related to the magnetic properties of the substances under investigation. Specifically, the absorption of radio frequency electromagnetic radiation by a sample subjected to an incredibly strong magnetic field (typically 7.04 Tesla) elucidates the bonding behavior and locale of protons in the sample due to the diamagnetic shielding associated with their electronic environments.

In the study of magnetic nanoparticles, several characterization methods have taken precendence. Mössbaur spectroscopy [32] is incredibly useful for confirming the results of XRD, TEM, and magnetometry as it is (1) keen to separate components of a multiphase system, (2) find magnetic moments of samples, and (3) study interactions among many particles. Based on AC susceptometry measurements, Mössbaur spectroscopy uses the absorption of gamma radiation which probes resonant energy levels of fine-particle samples. Time consuming sample preparation and purification as well as expensive equipment or extreme operating conditions (as with the cooled superconducting magnets in NMR), limit the usefulness of some of these methods of characterization of compounds. Although these examples provide a good overview of several spectroscopic techniques available today, they are by no means comprehensive as there are many other spectroscopy methods capable of disentangling the structure and interactions of materials.

## 2.3 Biomedical Applications

### 2.3.1 Current Uses

Magnetic particles offer the biomedical sciences unparalled sensitivity, customizability, and control in the development of immunoassays, biosensors, and fast diagnostic techniques [10]. Due to their relatively wide range of sizes, magnetic particles are well-suited for highly-specific biomedical applications such as single cell manipulation and cell-by-cell treatments. Their size and biocompatibilty also allow them to work on the inside as well as the outside of cells depending on their surface functionalization or interaction with cellular membranes. The areas of drug and gene delivery, biosensors, pathogen and cancer detection[19], and cell separation[10] have all seen substantial contributions from the nanotechnology sector. Xiaoquin et al. listed a great many uses of not only magnetic nanoparticles (magnetic capture and detection, giant magnetoresistive probes, and magnetic resonance contrast enhancement), but also the uses of quantum dots, nanofibers, and several other classes of nanoparticles [10]. Because biologically relevant engineered systems need to be unobtrusive as well as sensitive to the changes at the molecular level, the customizability of particles is accutely relevant to the next generation of biomedical technology.

### 2.3.2 Immunoassays

One particular method of probing the behavior of a biological system is through detecting and characterizing protains. As one of the four major biological components seen in nature and a critical element of many enzymes, structural materials, and disease markers, proteins are a strong choice in the selection of materials to focus the attention of this project. The immunoassays (antigen/antibiody couple-based detection schemes) and biosensor techniques currently used in biomedical laboratories have developed over many years of research and practical use in the lab. Currently, the three main subclasses of protein transfer methodolo-

gies reported are known as simple diffusion, vacuum-assisted solvent flow, and electrophoretic elution[22]. Western Blotting (electrophoretic elution) as seen in Fig. 2.3 (photo courtesy of *www.merckmillipore.com*) , a common immunoassay used for protein idendification, was reviewed by Kurien et al. [22]. This technique is based on the concept that proteins can be transferred to a membrane from a gel, post-electrophoresis, for further studies. It was noted that sensitivity to low protein concentrations, ease of preparation, and long-lasting results make Western Blotting a powerful technique in protein identification of multiple antigens simultaneously. One down side to this approach, however, has been the time required for sample preparation and post-processing, often employing several steps to extract and label the particular protein of interest. Cost and labor necessary to run a few protein types throug this system also make it a less attractive choice as new methods are developed. Although they are practical for most research purposes, these gel-based methods are not suitable for *in vivo* studies or the analysis of "contaminated" samples which contain compounds that may obscure the results or interfere with the preparation of a readable gel. A similar immunoassay, called ELISA 2.4, (photo courtest of *www.mitosciences.com*) does not use gels and electrophoretic mobilities of proteins to separate components of a system but rather the direct, specific, and strong coupling of immune system componenets (antigen/antibiody couples) deposited on the surface of a plate. ELISA suffers from similar difficulties as does Western Blotting in terms of labor and economicl restraints.

### 2.3.3 Magnetic Immunoassay Development

On the side of magnetic immunoassays, over several years Kotitz et al. [20] and Lange et al.[23] worked in the field of magnetorelaxometry in an attempt to study the binding reactions between avidin/streptavidin and biotinylated IgG/streptavidin using magnetic nanoparticles. Kotitz et al. [20] reported the first results of the analysis of the avidin-streptavidin system using magnetorelaxometry with which he observed a relaxation signal prortional to

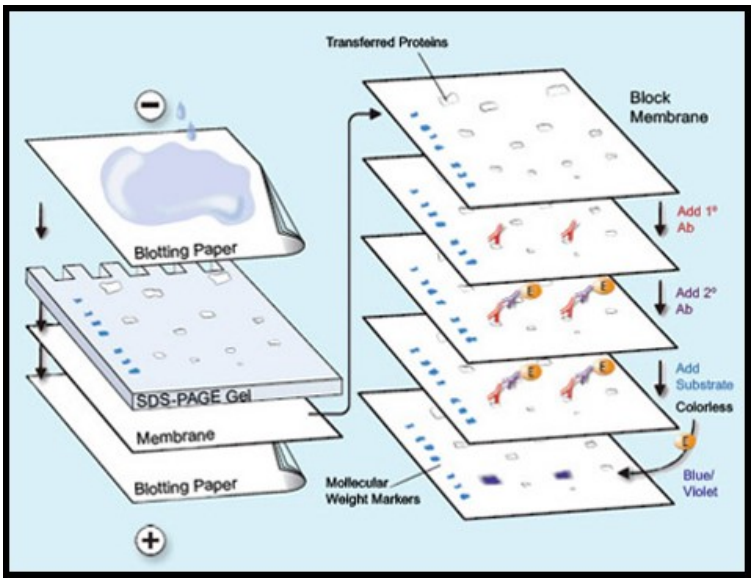


**Figure 2.3:** Western Blot (Immunoblot) uses antibody-protein interactions to bind substrates of interest after gel electrophoresis

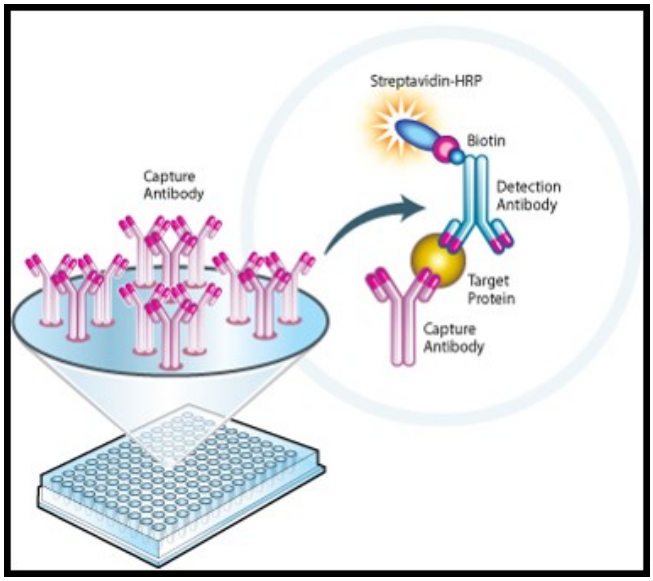


**Figure 2.4:** ELISA Immunoassay functional components including substrate and antigen/antibiody pair on a UV-Vis plate

the amount of avidin added until approximately 10 $\mu$g. The remanent behavior induced in the approximately 80 nm nanoparticles by the weak magnetizing fields of 1.6 kA/m for 1

second were subsequently measured using a dc-SQUID magnetometer. By carefully selecting the measurement window of interest based on particle size (see Section 1.1.2), they were able to determine that the Néel mechanism was the better relaxation method to quantify binding reactions over a wide range of concentrations since the rotational ability of the aggregated nanoparticles was effectively inhibited after a certain cluster size. Lange et al.[23] extended this work in the Weitschies group a few years later into the biotinylated IgG-streptavidin system to compare this novel immunoassay method with the ELISA assay. Although the detection limit of the magnetorelaxometry-based system was slightly less than that of the ELISA immunoasay, the results were comparable with the additional benefit of the SQUID based method exhibiting versatility of measurement conditions (for example, *in vivo* measurements and the lack of washing or separation steps).

As an extension of their work in magnetorelaxometry, the Weitschies group then expanded for several years into optical detection of transient birefringence effects in magnetic nanoparticle colloidal suspensions by studying the Cotton-Mouton effect [4, 13]. By enhancing the anisotropy due to the aligned particles in the field, a decaying birefringence was converted into changing transmitted light intensities. Compared to SQUID measurements, this technique required less extensive equipment to protect the sample and simpler data acquisition techniques, an improvement over previous work in magnetorelxometry for measuring the same binding reactions. For these studies, the magnetic nanoparticles were chosen so as to relax only according to the Brownian mechanism by using the larger fractions of separated particles with a mean diameter of 62-69 nm. These studies were carried out at magnetizing fields of 4.8 kA/m orthogonal to the direction of light propagation. Due to a knowledge of the relaxation mechanism, particle diameters could be determined according to Eq. (1.2). The increased first-order decay relaxation time observed was due to the aggregation of the mangnetic nanoparticles by the coupling reaction of mono and polyclonal antibodies through the streptavidin-biotin binding reaction. Only the polyclonal antibody

system, capable of crosslinking different particles together to form larger clusters, showed any significant increase in relaxation time. This was due to the fact that the antibodies could bind to several different epitopes on a single antigen, allowing aggregation of the particles to occur.

Limitations of this system reported were the applicability of magneto-optical birefringence measurements to only those systems relaxing according to the Brownian mechanism since Néel relaxation does not cause a change in birefringence at the pertinent time-scale, as well as problems associated with the scattering and absorption of the laser beam. Later, this system was used to study a kinetic, stepwise polymerization model of the aggregating nanoparticles to compare to SPR measurements. Limits of detection of $\sim$1 pmol/mL and $\sim$70 fmol/mL were reported for the biotinylated hEotaxin and IgG antigen systems, respectively. Overall, it was reported that this novel system was more clinically relevant than previous relaxation models since it was not prone to external disturbances, although its sensitivity regarding the magnetic signal was reduced.

### Most Recent Development of Birefringence Based Functionalized Nanoparticle Size Determination for Magnetic Immunoassays

In the years since the work of Weitschies and others in the magneto-optic and magnetometric regimes, a series of studies took place that took magnetic immunoassay development to a whole new level. The understanding that the vibrational behavior of particles in suspension could be coupled to the size of the particles and that this could act as a characterization technique prompted Ku et al. to develop a birefringence-based immunoassay technique [21]. In their study, Ku et al. used a Debye relaxation model to predict the frequency behavior of particles rotating in ferrofluids under the application of an external field of 4.8 kA/m (to be probed by a linearly polarized laser beam, as in Faraday Rotation studies):

$$\sigma(\omega) = \frac{\sigma_o}{1+\omega^2\tau^2} - i\omega\tau\frac{\sigma_o}{1+\omega^2\tau^2} \tag{2.3}$$

where $\omega$ represents the circular frequency of the periodic process (forcing frequency) and $\tau$ represents the time constant of the behavior. It was the changes in this time constant as a function of frequency that became the crucial discovery of this study. The first term in Eqn. 2.3 is the real component (in-phase response) and the second is the imaginary (out-of-phase repsonse).

A peak was expected in the out-of-phase response at a critical frequency corresponding to the rotational diffusion time of the magnetic particles (based on size), as in Eqn. (2.4). Brownian rotation was the only siginificant relaxation method at the sizes tested by Ku et al., as confirmed by Kotitz et al. [20] in Fig. 1.2.

$$f_p = \frac{3k_BT}{\pi^2\eta D_h^3} \tag{2.4}$$

where $D_h$ indicates the hydrodynamic diameter of the rotating particle. For an optical setup, both a crossed polarizer with single photodetector approach as seen in Fig. 2.5 and an offset waveplate with balanced photodetector approach in Fig. 2.6 were studied. It was shown that the latter option gave a smaller noise floor and a greater signal-to-noise ratio and was thus preferred.

The in-phase and out-of-phase responses expected shown in Fig. 2.7 gave a full picture of the behavior of the nanoparticles studied with a peak at the expected location. This thus confirmed the hypothesis that the birefringence was probably caused by a single predominant anisotropy-inducing factor: the Brownian rotation of the nanoparticles. Ku et al. used approximately 98 nm (hydrodynamic diameter) antibody functionalized particles at 0.004 V% for their study and were able to detect differences in sizes down to 7.8 nm as see in Fig. 2.8 based on the frequency shift of the peak as the overall sizes increased [21]. One concern

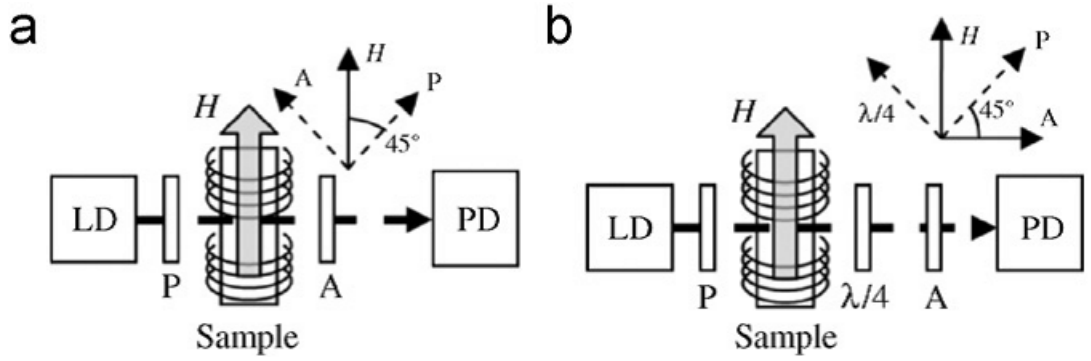


**Figure 2.5:** Simple crossed polarizer setup for birefringence particle studies [21]

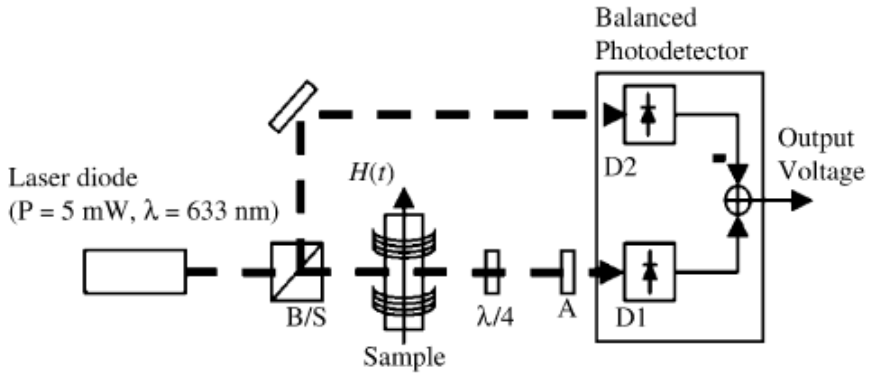


**Figure 2.6:** Improved polarizer setup for birefringence particle studies [21]

as the particle sizes increased was a broadening of the peak used to characterize them. This was interpreted as the broadening of the size distribution of particles as dimers or chains may have formed with the addition of the final antigen layer to the test ferrofluid.

Magnetic measurements using magneto-optic effects as well as magnetorelaxometry have been advancing dramatically in recent years. The faraday rotation is a well-studied, robust phenomenon capable of sensitive detection in nearly all transparent crystalline, liquid, and colloidal systems. Limitations are usually encountered in the form of low amplitude responses for materials with small verdet constants, but there are methods available to address this such as optical cavity enhancement. These studies also show how magnetic particles have

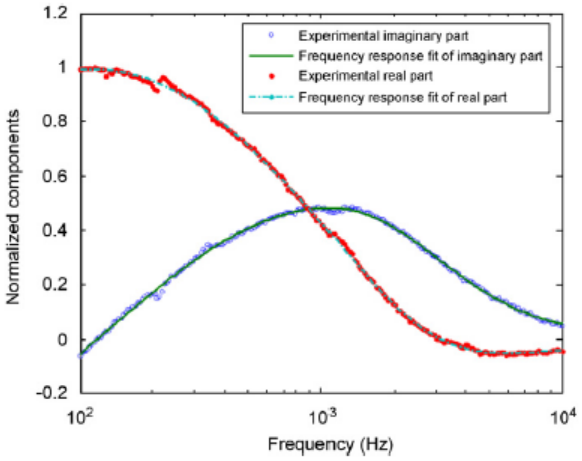


**Figure 2.7:** Initial results in birefringence studies (background subtracted, normalized components) [21]

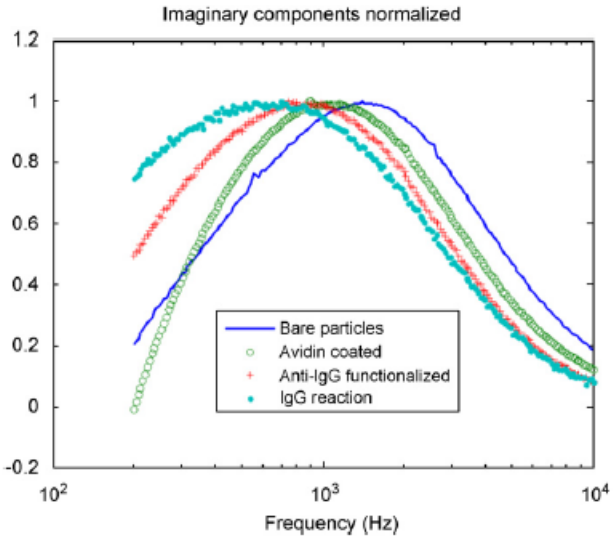


**Figure 2.8:** Initial results in birefringence studies for functionalized layers (background subtracted, normalized components) [21]

been used in the literature as sensors for biological reactions. One major challenge has been balancing the sensitivity of specific measurement systems with their universality, all the while advancing toward techniques capable of being used in a clinically-relevant environment.

## 2.4 Direction of Research

Given these advances in current nanomedicine, there is still room for improvement in immunoassay development. The goal of the proposed work is to replace or complement Western Blotting and ELISA in the biomedical laboratory with a more effective, universal, and efficient magneto-optical method of protein characterization based on the most recent work of Ku et. al [21]. An improved system is to be developed with greater versatility in measurement and larger signal-to-noise ratio. It is the purpose of this study then to (1) eliminate or minimize the need for costly reagents and biomarkers and (2) reduce the currently long preparation and incubation times while maintaining the sensitivity and reproducibility developed over many years of gel-based technique improvement. Other potential benefits of the proposed solution is the development of new small volume viscometers, single surface biological functionalization vibration measurements, and Dynamic Light Scattering (DLS) technologies based on the travel of magnetic particles in a fluid of interest.

# CHAPTER 3: METHODOLOGY

## 3.1 Faraday Rotator Cell Development

### 3.1.1 Electromagnet

To explore the interaction between light and magnetized materials, a strong magnet was developed. The setup for this work involved an approximately 300-turn electromagnet of 11 Gauge copper wire enveloping a 12.7 mm aluminum tube with an air core, versatile enough to accommodate any material of interest, as seen in Fig. 3.1 and Fig. 3.2. The current air-core design is capable of fields up to approximately 700 kA/m (0.07 Tesla) at a DC current of 12 Amps.

At higher currents heating from the 15+ layers of coils becomes an issue. For some of the proposed experiments, a higher field of at least 0.1 T was required, so an enhanced design involving core materials was involved. Specifically, two 44.45 mm long highly permeable HiMu80 cores were machined with a 3.66 mm center bore to magnify and uniformize the field in the region of interest. Preliminary measurements indicate that with a 6.60 mm separation of the cores, enough to accommodate sample cuvettes of 2.8 mm width, a max uniform field of 0.28 Tesla was achieved. This was measured using a AlphaLab Model GM-2 Gaussmeter with a resolution of 0.1 G. Even larger fields could theoretically be produced with smaller separations and heat treated HyMu80 material. As an additional benefit, the near-negligible Faraday Roatation due to the air-core portion of the core was mitigated with the confinement of the flux density in the annular region of the HyMu80 cores. By varying the sample and core locations, a wide range of constant or spatially varying fields were attained for future studies as seen in Fig. 3.3. For this project, a constant field along the direction of the propagation of the polarized elliptically-shaped beam was chosen to minimize spatial

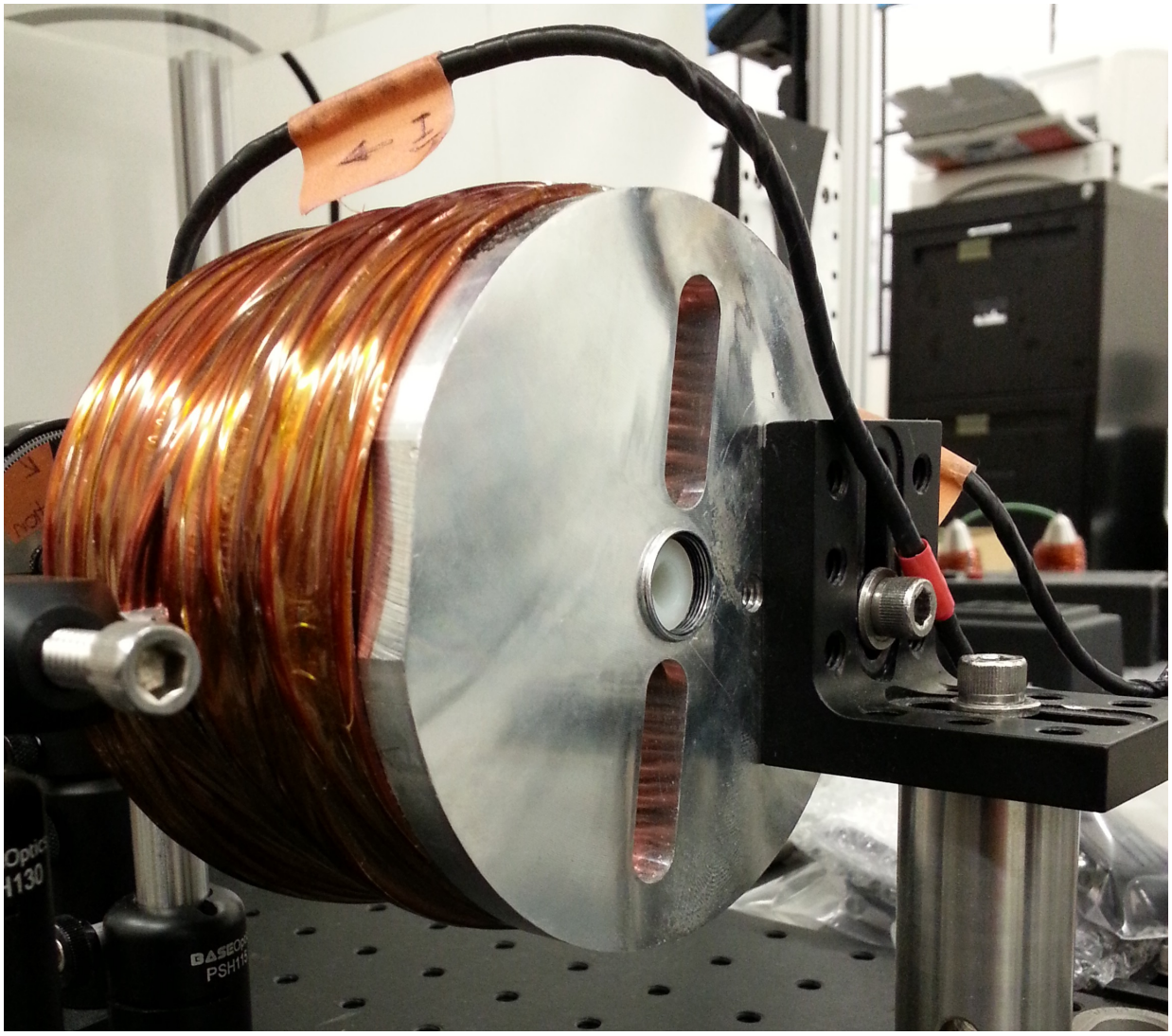

**Figure 3.1:** Machined 300-turn 0.1 T electromagnet used in experiments

difference errors along the sample.

The experimental cell placed at the center of the electromagnet between the two HyMu80 pieces was accessible to the light, shielded from external fields, and isolated from optical disturbances by its location. Given the dimensions of the experimental cell, a separation of 6.60 mm and a field of approximately 600 Gauss was measured and used for the in-phase field component in AC studies. Without a highly permeable core, the field strength measured

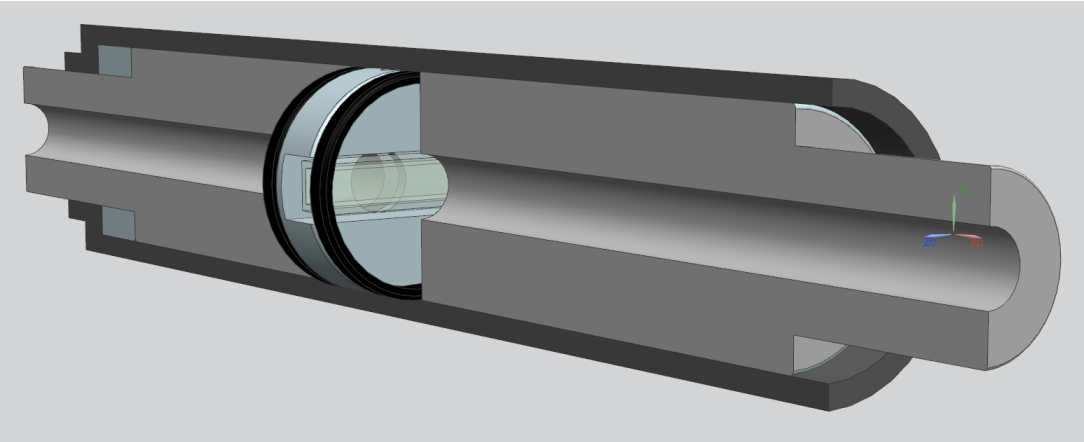

**Figure 3.2:** Proposed Faraday Rotator Cell design with included core components. A 2.8 mm fluid cell was assumed with a 6.60 mm core separation

drops to 167 Gauss. Given the needs of a particular measurement, the HyMu80 cores were used in some cases and not in others. The main reason for this was the need to uniformize the experimental responses for high frequency fields and to determine the dependence of time-domain responses to core permeability and magnetic isolation.

### 3.1.2 Sample Holder and Cuvette

The sample cuvettes to be used are borosilicate glass capillary tubes (Wale Apparatus, Model S-102) with wall thickness of 0.4 mm and a pathlength of 2 mm as shown in an "exploded view," and assembled view, and an electromagnet and water loaded view in Fig. 3.4. Although the electromagnet core can acccomodate large samples and pathlengths of up to 76.2 mm, the miniturization of required sample volumes is of great interest to the development of sensitive immunoassay techniques. Additionally, light scattering and reflection due to solvent inhomogeinities and nanoparticle/bead interference are minimized with short sample pathlengths.

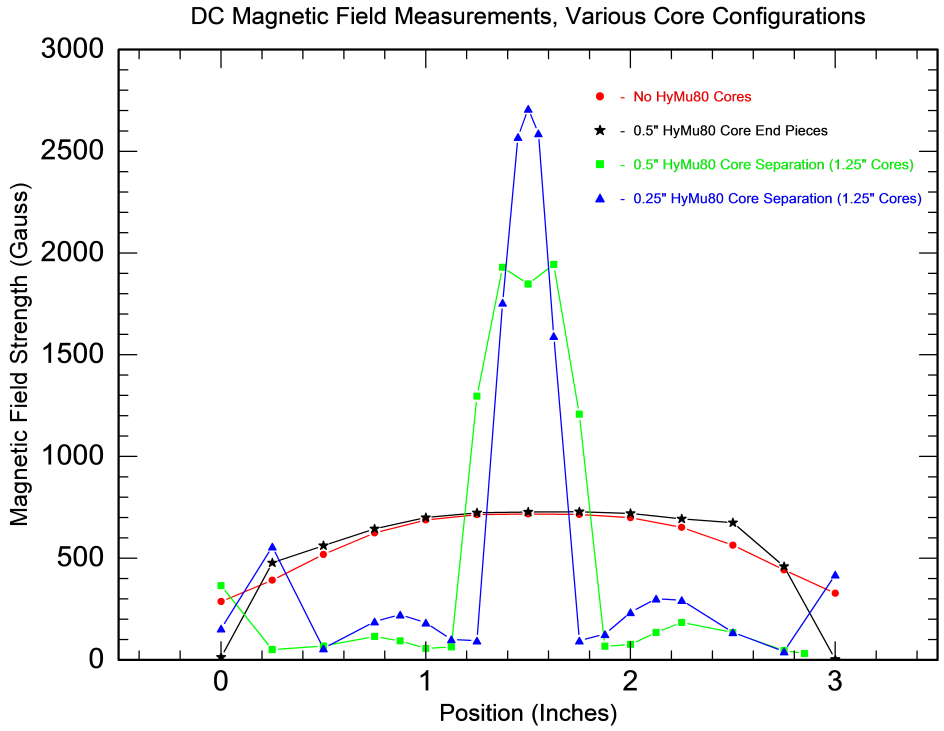


**Figure 3.3:** Dependence of magnetic field strength on the separation of HyMu80 cores

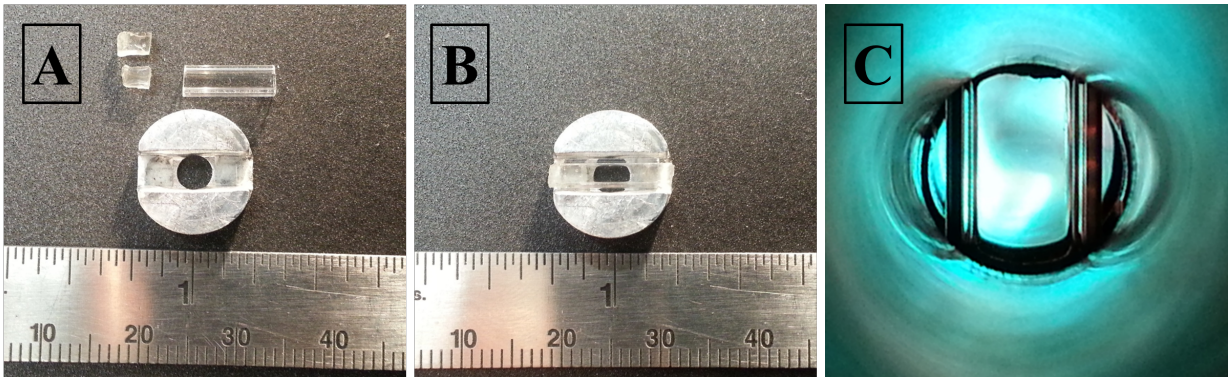


**Figure 3.4:** Borosilicate glass cuvette and aluminum holder with internal view of light path through solenoid core

## 3.2 Laser and Optics

In studying the magneto-optic Faraday rotation, a 3 mW diode laser system was implemented. Designed to output laser at a wavelength of 785 nm, this diode the faraday rotation

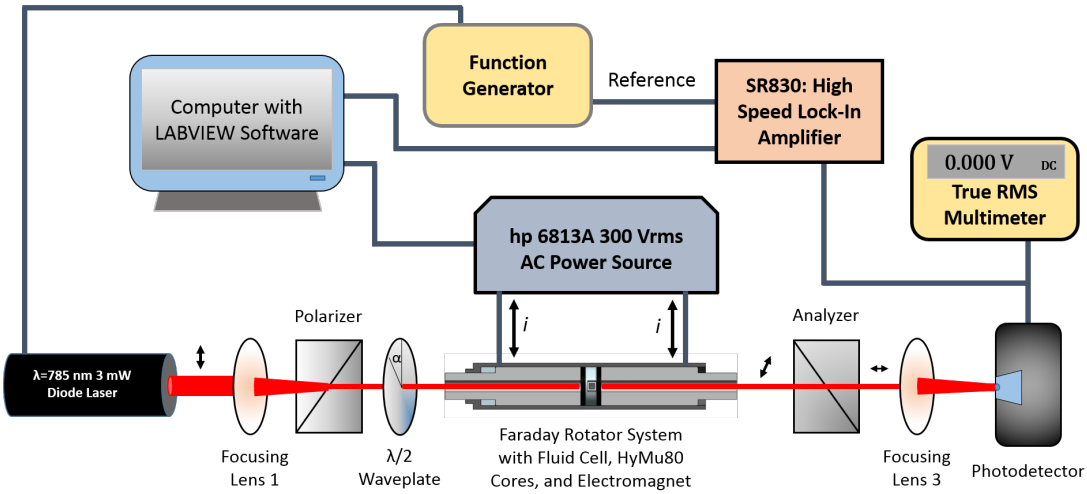


**Figure 3.5:** Original experimental setup of the optical bench system used in faraday rotation experiments with a single diode

of a sample can be measured precisely at one location of the electromagnetic spectrum. Future studies can focus on the behavior of such as system under varying wavelengths using the Chameloen Femtosecond Laser acquired by the laboratory. To attain a continuous laser pulse, a lock-in amplifier (Stanford Research Systems SR830) determined the intensity of the laser directly through voltage control. Originally, a single beam and photodiode with a nearly crossed polarizer setup and a half waveplate was used to measure Faraday Rotation responses. This was the simple system tried by Ku et al. as seen in Fig. 2.5 and modelled similarly for early experiments in faraday rotation for this project in the diagram shown in Fig. 3.5. Due to its simplicity, this model was a good first choice for DC faraday rotation measurements. Fig. 3.6 and Fig. 3.7 show the most recent optical bench system set up similarly to that used by Ku et al. as an improvement over the simple crossed polarizer system.

The optical elements included in the newest model include (from the laser source) a focusing lens to collimate the incoming beam, a Glan-Taylor polarizer to linearly polarize the circularly polarized source, and an electromagnet with sample and magnetic field control. On

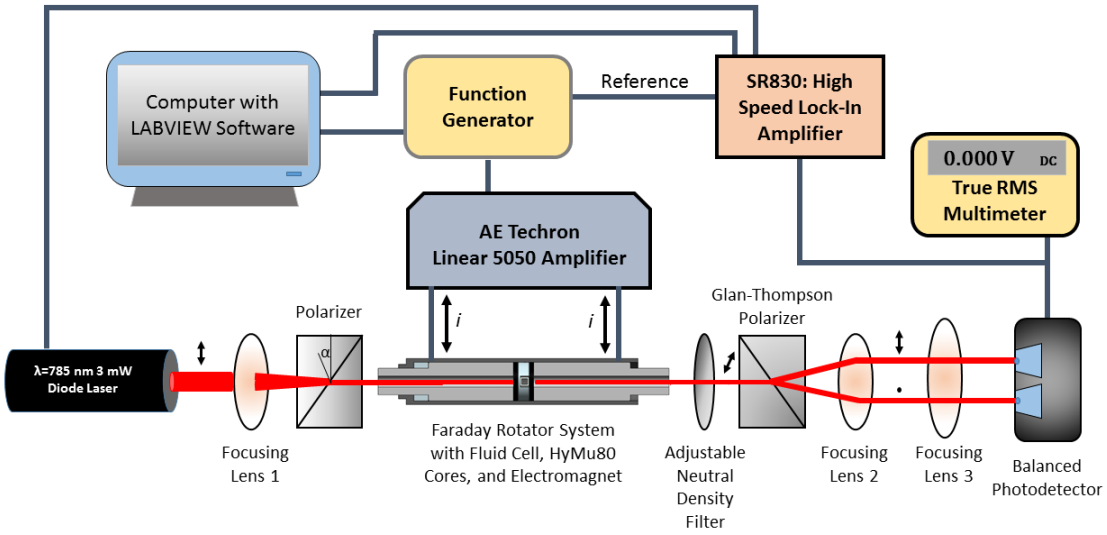


**Figure 3.6:** Latest experimental setup of the optical bench system used in faraday rotation experiments with a balanced photoddetector and no waveplate

the other side of the electromagnet, a Glan-Thompson polarizer split the p and s polarizations and directed them at 45 degrees to each other. This allowed a differential measurement to be taken betwen the two changing polarizations as the faraday rotation took effect. Additionally, Ku et al. [21] noted how the noise floor for this system was much lower due to the polarizer fast axes set at 45 degrees relative to each other to produce a region of highest intensity of light to take a differential measurement. Laser shot noise (quantified and compared by Ku et al. [21]) was not a major problem with this optical setup.

## 3.3 Measurement System High-Frequency Analysis

In the proposed experiment, both AC and DC fields were used, with a function generator (Stanford Research Systems Model DS345 30MHz Synthesized Function Generator) and lock-in amplifier (Stanford Research Systems Model SR830 DSP Lock-In Amplifier) controlling

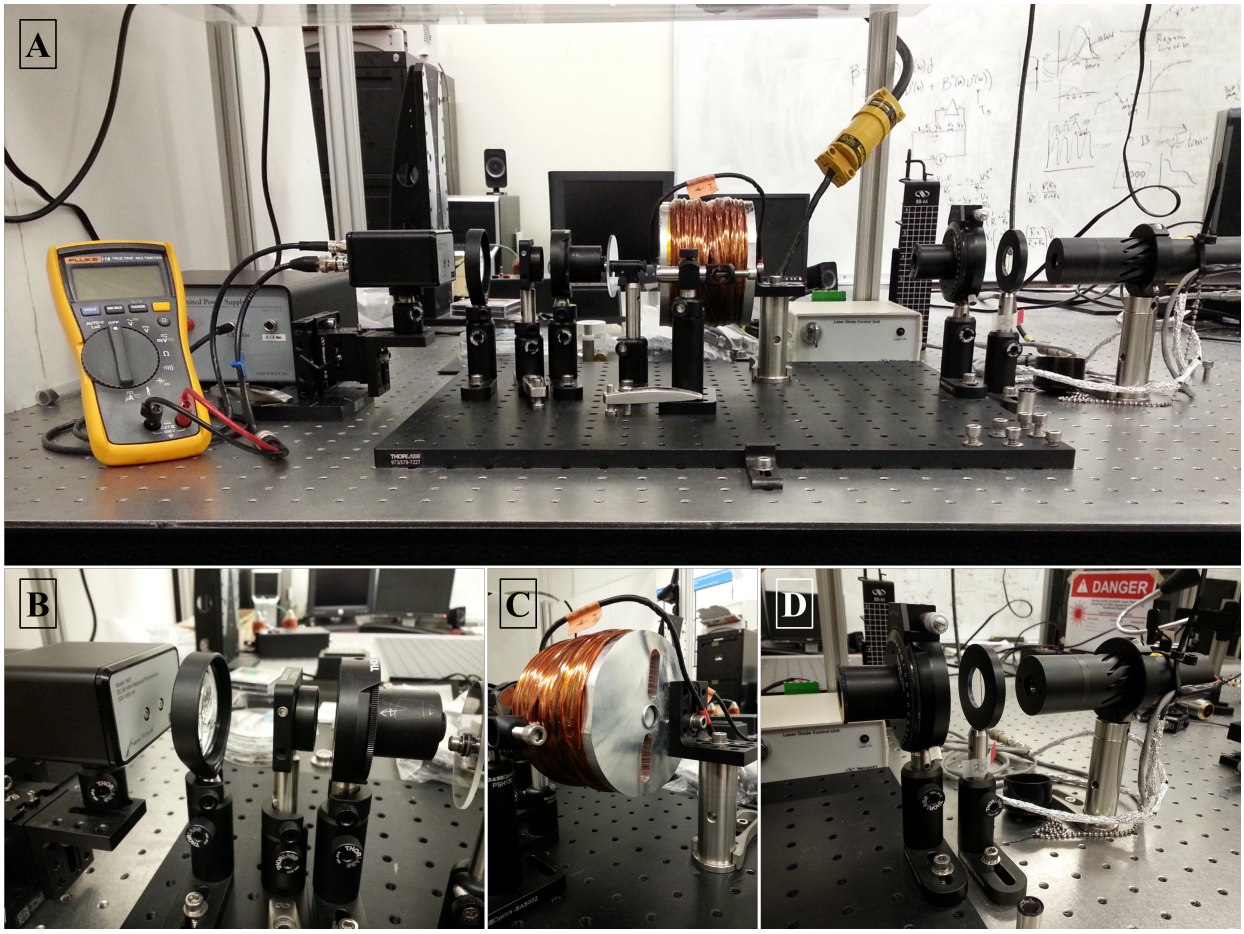


**Figure 3.7:** Experimental setup of the laser system used in faraday rotation experiment. A) Optical bench components arranged in series. B) Optical elements after the sample including a neutral density filter (variable), a Glan-Thompson polarizer, and a series of focusing lenses before a Balanced New Focus Photoreceiver. C) Electromagnet with teflon spacers for sample placement. D) Optical elements before the sample including the laser source 785 nm, a focusing lens, and a Glan-Taylor polarizer

and processing the waveforms (sine or square) and signals developed. For AC measurements, a function generator was used to vary the input modulation from DC conditions up to 20 kHz on an hp 6813A AC Power Source/Analyzer for DC fields (and low frequency AC fields) and an AE Techron 5050 Linear Amplifier for AC fields. A DC field was produced with an hp 6031A 20V, 120A, 1000W System Power Supply that maintained a field strength corresponding to 12A peak current (2637 Gauss). For data acquisition, a custom LabView program was developed capable of taking measurements under both DC and AC conditions

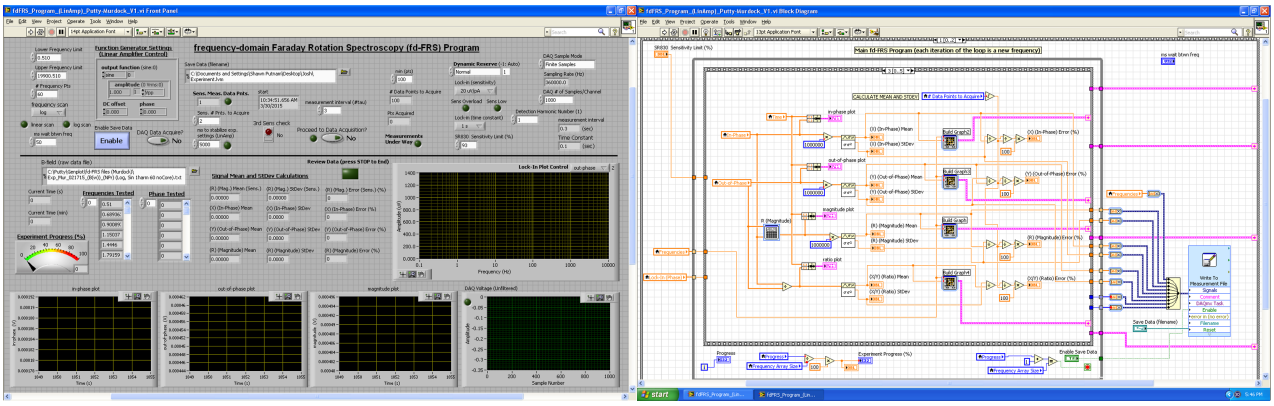


**Figure 3.8:** LABVIEW Program developed for DC and AC conditions capable of reading data from GPIB output of Lock-In Amplifier at 512Hz max and locking onto 0.001 Hz to above 30 kHz

and scanning through the entire spectrum of wavelengths and driving frequencies (see Fig. 3.8). For the AC measurements, the Lock-In Amplifier was able to use the TTL output of the Function Generator as a reference on which to lock and a computer was used to gather and store the data.

Due to several key limitations, a setup similar to the work of Pagliero et al. [26] requiring the use of an optical cavity enhancement of faraday rotation did not form a part of the initial experimental setup. Specifically, the reduced signal amplitude caused by a single pass of the beam through the cuvette was be offset by higher field strength oscillations, high frequency lock-in amplifiers, and carefully controlled environmental conditions to process the signal of interest and reduce background noise during data acquisition. Another possible addition to the experimental setup that was not successfully implemented was the active locking of the lock-in reference to the actual magnetic field through the use of a high frequency magnetic field probe. A locking and amplification circuit was attempted using a Zener Diode and Op-Amps, but without success as the signal from the Gaussmeter probe was far too noisy and small.

## 3.4 Derivation of the Verdet Constant from the Measured Faraday Rotation with Phase Lag Calculations

In the measurement of faraday rotation signals corresponding to the rotation of polarized light, a series of calculations related to the derivation of the expected rotations was conducted as shown below in Eqn. 3.1 to 3.18, depending on the case: with or without magnetic field phase lag. Both scenarios are discussed in the following section.

### 3.4.1 Dynamic Function Generator to Linear Amplifier Signal with No Phase Lag Correction

Under ideal conditions, as stated earlier, Faraday's Law states:

$$\theta = B\nu l \tag{3.1}$$

In the case of AC field oscillations, a frequency dependence is expected for each term. The magnetic field is directly oscillated using a power supply or an amplifier. This, controlled by a function generator (internal or external to the field source) determines $\omega$. The pathlength, l, is expected to exhibit such a weak frequency dependence that it is essentially constant for the purposes of this work. $\Theta$, representing the theoretical faraday rotation, is expected to follow the driving frequency in-phase entirely, given ideal conditions and no electronic lag.

$$\theta(\omega) = B(\omega)\nu(\omega)l(\omega) \tag{3.2}$$

Corresponding to the response of the rotation of light is a voltage change on the balanced photodiode given by

$$V(\omega) = V(\omega)^{real} + iV(\omega)^{imag} \tag{3.3}$$

By using a sine wave as a forcing waveform and calibration curve for the optical sensitivity of the system, a new expression for $V(\omega)$ can be obtained.

$$V(\omega) = \theta(\omega)[\sqrt{2}(\frac{dV}{d\theta})] \tag{3.4}$$

Incorporating Eqn. 3.2 and Eqn. (3.3) into Eqn. (3.4), one obtains

$$V(\omega)^{real} + iV(\omega)^{imag} = [\sqrt{2}(\frac{dV}{d\theta})]B(\omega)l(\nu(\omega)^{real} + i\nu(\omega)^{imag}) \tag{3.5}$$

The real and imaginary (In-phase and Out-of-Phase) components of this system are shown in Eqn. (3.6) and Eqn. (3.7).

$$V(\omega)^{real} = [\sqrt{2}(\frac{dV}{d\theta})]B(\omega)l\nu(\omega)^{real} \tag{3.6}$$

$$V(\omega)^{imag} = [\sqrt{2}(\frac{dV}{d\theta})]B(\omega)l\nu(\omega)^{imag} \tag{3.7}$$

Solving for $\nu$, the real and imaginary components of this material property can also be determined in Eqn. (3.8) and Eqn. (3.9). This method of analysis allows a material property to be used as the determinant of the faraday rotation in ideal AC conditions. Note that Ku et al. [21], whose system closely resembled the one in this work, used birefrinegence instead of Verdet constant for their analysis. This method is new and likely to yield more than a single peak corresponding to all of the anistropies due to the vibrations, rotations, inverse faraday effects, etc. related to the change in birefringence and other properties of the sample at different critical frequencies, such as the one derived in as derived in Eqn. (2.4).

$$\nu(\omega)^{real} = \frac{V(\omega)^{real}}{[\sqrt{2}(\frac{dV}{d\theta})]B(\omega)l} \tag{3.8}$$

$$\nu(\omega)^{imag} = \frac{V(\omega)^{imag}}{[\sqrt{2}(\frac{dV}{d\theta})]B(\omega)l} \tag{3.9}$$

### 3.4.2 Magnetic Field Phase Lag Correction Case

In the case that the magnetic field is lagging behind the forcing frequency of the Function Generator or the AC Power Supply, a more complex analysis must take place as shown. The frequency dependence of the faraday rotation is first assumed

$$\theta(\omega) = \theta(\omega)^{real} + i\theta(\omega)^{imag} \tag{3.10}$$

Similar to the case with no phase lag, all components of Faraday's law are assumed to have a frequency dependence, except for the pathlength.

$$\theta(\omega)a^{real} + i\theta(\omega)^{imag} = B(\omega)l(\nu(\omega)^{real} + i\nu(\omega)^{imag}) \tag{3.11}$$

$$\theta^{real} + i\theta^{imag} = (B(\omega)^{real} + iB(\omega)^{imag})l(\nu(\omega)^{real} + i\nu(\omega)^{imag}) \tag{3.12}$$

An adjustment phase correction (corresponding to the phase lag of the field, measured with a high frequency Gauss probe) is then applied to the field using Euler's Formula and then expanded

$$B(\omega)^{adjusted} = Be^{-i\phi} = B[cos(\phi) - isin(\phi)] \tag{3.13}$$

$$B(\omega)^{adjusted} = [B(\omega)^{real} + iB(\omega)^{imag}][cos(\phi) - isin(\phi)] \tag{3.14}$$

$$B(\omega)^{adjusted} = B(\omega)^{real}cos(\phi) - iB(\omega)^{real}sin(\phi) + iB(\omega)^{imag}cos(\phi) - i^2B(\omega)^{imag}sin(\phi) \quad (3.15)$$

$$B(\omega)^{adjusted} = B(\omega)^{real}cos(\phi) - iB(\omega)^{real}sin(\phi) + iB(\omega)^{imag}cos(\phi) - i^2B(\omega)^{imag}sin(\phi) \quad (3.16)$$

From this analysis, the new, adjusted real (in-phase) and imaginary (out-of-phase) components of the field can be expressed in terms of the phase lag and original in-phase and out-of-phase magnitudes

$$B(\omega)^{real,adjusted} = B(\omega)^{real}cos(\phi) + B(\omega)^{imag}sin(\phi) \quad (3.17)$$

$$B(\omega)^{imag,adjusted} = -B(\omega)^{real}sin(\phi) + B(\omega)^{imag}cos(\phi) \quad (3.18)$$

Application of the solution of the complex system of Eqn (3.17) and Eqn (3.18) for $B(\omega)^{real}$ and $B(\omega)^{imag}$ and inserting these into Eqn (3.16) yields the result that the $B(\omega)^{real}$ is the same as the $B(\omega)$ term in Eqn 3.7 (i.e. the magnitude of the magnetic field). The imaginary component can be shown to be zero for all $\omega$ for a properly phase adjusted system. This depends entirely on the quality of the interpolation used or the ability to actively adjust the phase of the measurement relative to the field lag at that instance. With this adjustment, even a system that is lagging can be locked onto properly to obtain phase-dependent data. Additionally, all signals measured with the Lock-in Amplifier must be corrected before insertion into the expression for the verdet constants given above in (3.8) and (3.9). The additional phase lag caused by material effects is then the only theoretical

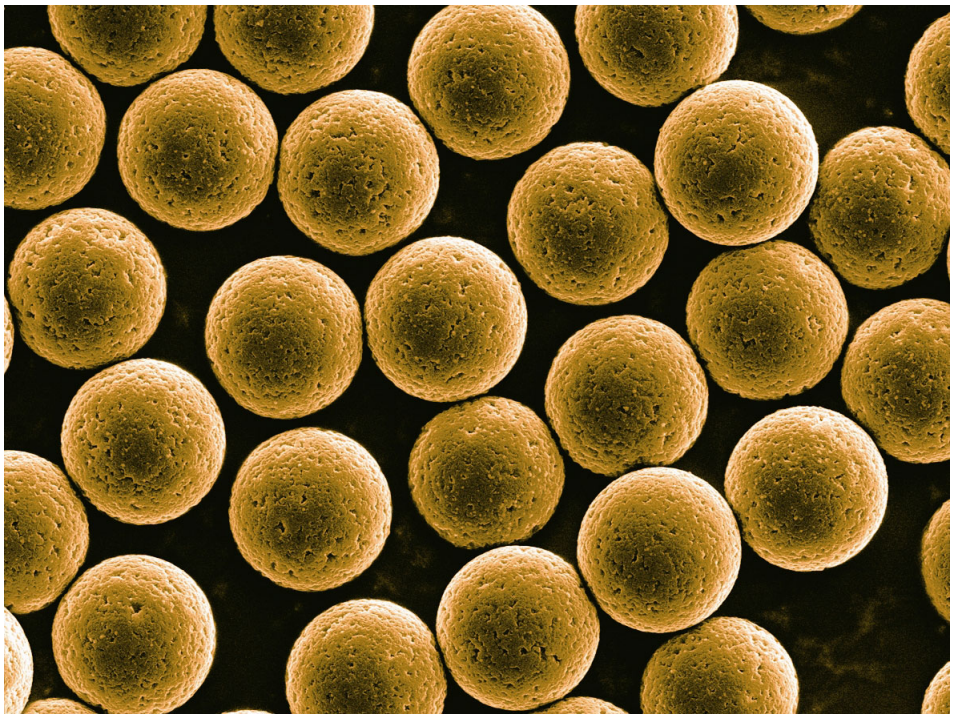

**Figure 3.9:** Industrially produced ferric oxide Dynabeads. Photo courtesy of *www.dddmag.com*

out-of-phase response of the measurement.

## 3.5 Particle Synthesis and Characterization

The particles used in this project fell into two categories: 1) in-house produced ferric oxide nanoparticles in the range of 200 to 500 nm and 2) commercially purchased ferric oxide Dynabeads of 1 $\mu$m in diameter as seen in Fig. 3.9, Fig. 3.11, and Fig. 3.10.

The in-house produced particles were characterized by Dynamic Light Scattering and showed a fairly large size distribution, with peaks indicated in Fig. 3.12 and Table 3.1.

### 3.5.1 Proposed Systems Studied and Experimental Methodology

For proof of concept and system development/calibration, the AC field magneto-optical resonant faraday rotation spectra of a 10 mm long Terbium Gallium Garnet (TGG) crystal

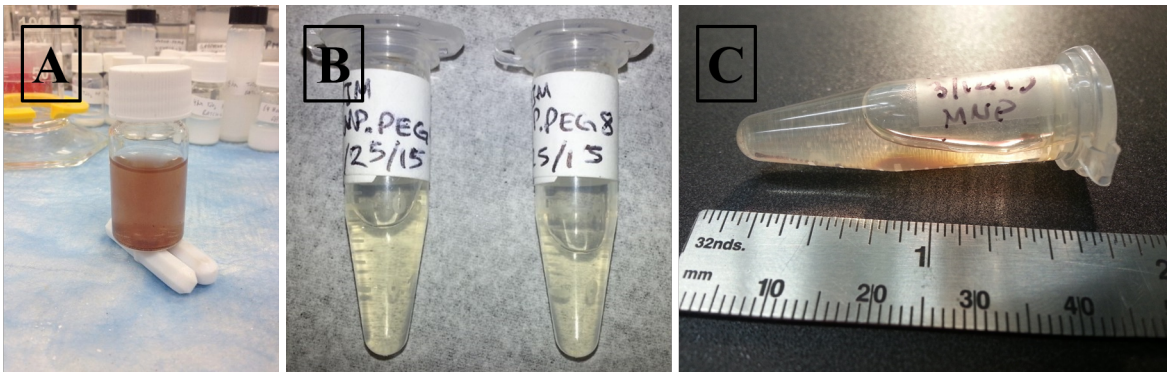


**Figure 3.10:** MNP samples showing monodispersity/stability and aggregation at different concentrations and settling times

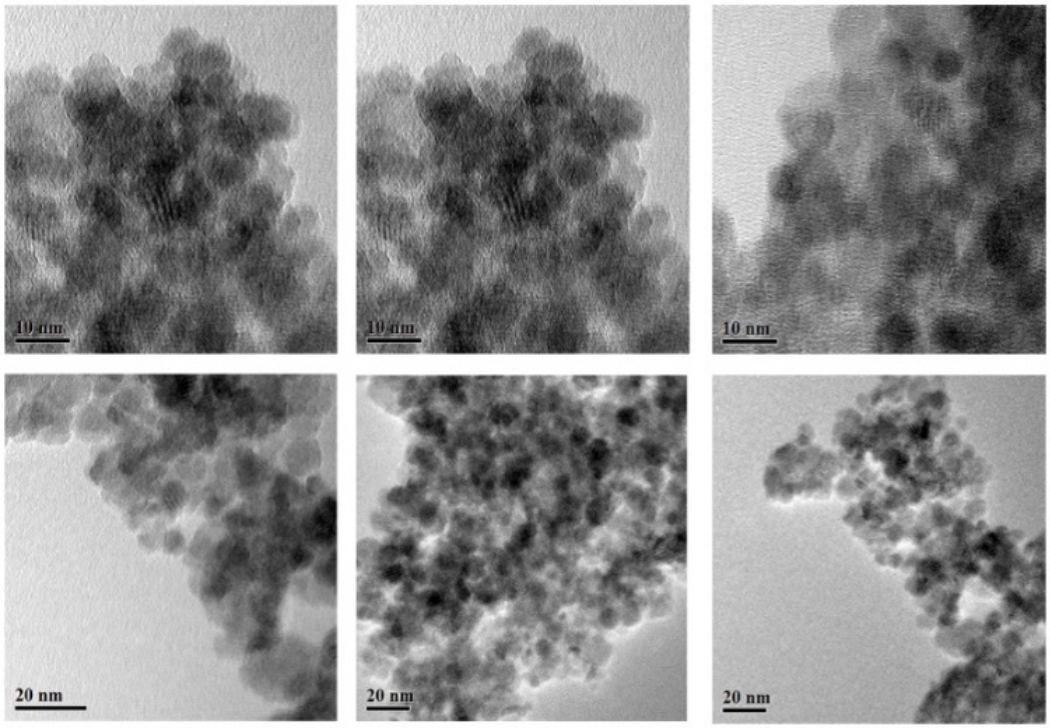


**Figure 3.11:** Transmission Electron Micrograph of aggregated in-house produced nanoparticles

(Northrup Grumman Synoptics, T0396), NBK7 glass sample, and pure water have been studied. Well defined through years of research, these systems will provide the noise quantification and system limits of detection for solid phase and pure liquid samples. Once these

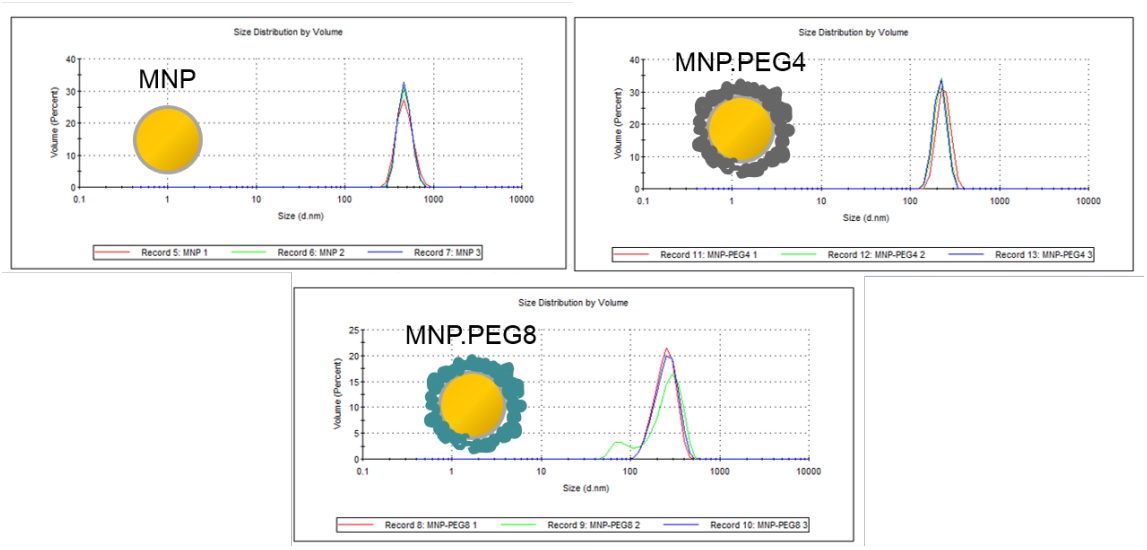


**Figure 3.12:** Dynamic Light Scattering characterization results for the bare and functionalized magnetic particle samples produced in-house

**Table 3.1:** Characterization Data for MNP samples from Seal Lab. The peak frequency was calculated from theory and conditions for water (Room temperature and viscosity of pure water at room temperatrure

| | Size, $D_h(nm)$ | Expected Peak Frequency, $f_p$(Hz) | Zeta Potential, Z $(mV)$ |
|---|---|---|---|
| MNP | 482.0 | 12.81 | 10.8 |
| MNP.PEG4 | 238.0 | 138.81 | -29.5 |
| MNP.PEG8 | 250.5 | 80.52 | -30.4 |
| Dynabeads | 1000.0 | 1.40 | – |

spectra were determined, Streptavidin Coupled Dynabeads (Life Technologies, Trial Kit 65801D) and magnetic nanopaeticles conjugated with surface functionalizations were studied. Used in a multiplicity of studies in cellular and biomolecular separation immunoassays, Dynabeads are well known in the biomedical sciences as a staple in translational nanotechnology products of high quality. Uniform in size, these iron oxide core, polymer shell beads allow for surface functionalization with nearly any biomolecule of interest. In addition to their stability in solution and multiple possible surface functionalities, Dynabeads are also shown to be superparamagnetic in nature, thus allowing studies into the magnetization of

nanoparticle/bead systems in an aqueous environment and their corresponding Brownian relaxation mechanisms.

Because of its ubiquitous presence in many studies on antibody-antigen binding reactions, the streptavidin/biotin coupling system was a safe place to start protein interaction studies ias desired in the use of Dynabeads. 1 $\mu$m particles coupled with streptavidin were characterized using the AC field system to prevent aggregation on one side of the fluid cell due to their magnetic separation capabilities for which they are prepared. Because of their medical significance, the characterization of proteins and their interactions is a viable extension into and contribution to nanomedicine. Although this work did not address these specific applications in practice, future work is clearly directed towards this goal.

# CHAPTER 4: EXPERIMENTAL RESULTS

## 4.1 Steady State DC Field Results

### 4.1.1 Results with Distilled Water and TGG

In an effort to understand the underlying phenomena of faraday rotation in various samples and prepare the measurement systems currently available, a well-known material was tested under DC conditions: Distilled Water, Double Deionized (DDW), the major solvent for most biological reactions.

In Fig. 4.1, the most recent results for the faraday rotation of water is shown along with a calibration curve. The positive and negative rotation data points correspond to positive and negative magnetic fields applied in DC conditions. Positive fields were defined to be in the direction of light propagation and vice versa for negative field values. It should be noted that the observed rotations are symmetric in nature and of significant magnitude so as to be accurately detected by the lock-in amplifier. The calibration curve exhibited a linear curve fit with an $R^2$ value of >0.999. One important limitation of these results was that, although the contribution of the borosilicate glass cuvette was subtracted out, the distilled water was not de-gased, nor was it purified to remove ions and other impurities for the early experiments. The extent of these sources of error are evident in Fig. 4.2. For the purpose of preliminary results, the interpolating function determined by Villaverde et al. was extended with some reservation to near IR wavelengths [36]. As shown in Fig. 4.2, future studies with the wavelength tunable femtosecond laser will be able to reproduce this data between 720-980 nm. It can be seen that the experimental data point corresponding to $\lambda$=785 nm is higher than that expected for pure water. Although the error in measured voltages were seen to have a mean uncertainty of 0.606%, the difference between the measured and literature

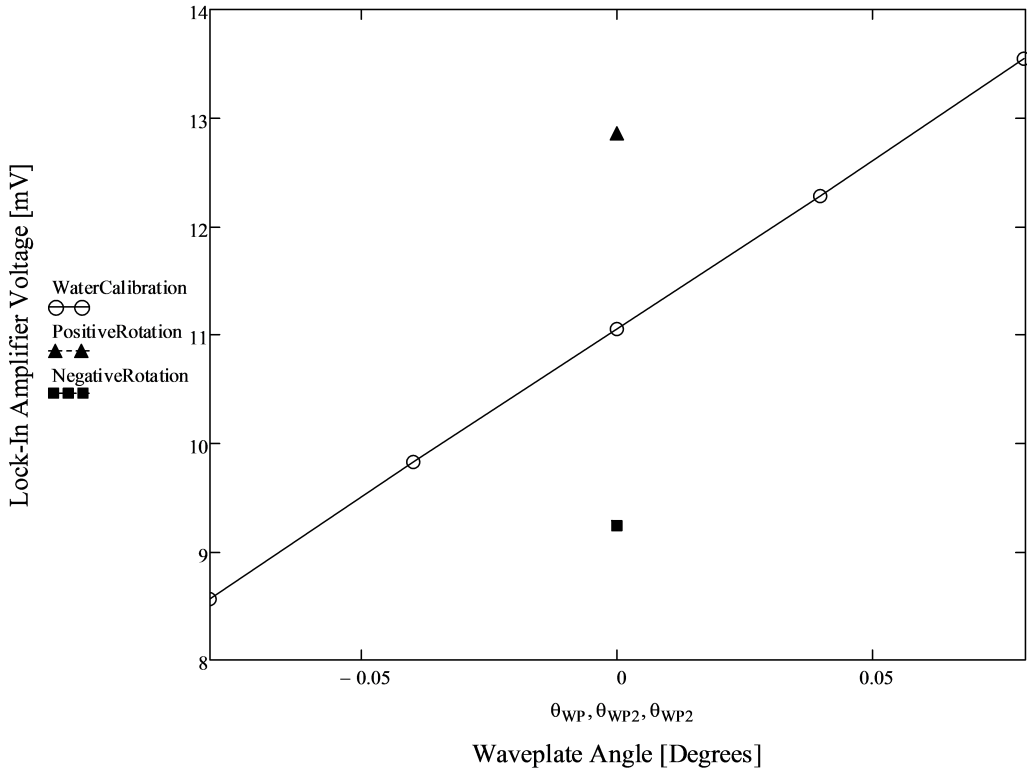


**Figure 4.1:** DC magnetic field faraday rotation results for distilled water in a fluid cell of a 2 mm pathlength. The laser beam wavelength was $\lambda$=785 nm with a pulsed frequency of 4850Hz. Magnetic field strength was measured to be an average value of 0.2637 Tesla over the sample region. A Lock-In Amplifier was used to measure photodiode response. N=5 for all conditions.

values can be easily explained by the foregoing explanation of sample impurity. Future experiments will also facilitate the use of purified sample systems.

## 4.2 Frequency Dependent Spectrum AC Field Results

### 4.2.1 Frequency Domain AC Magnetic Field

To show how well the phase lag correction derived earlier works, Fig. 4.3 and 4.4 show the results obtained for the correction applied to the magnetic field itself as if it were faraday rotation data. It can be seen that the first of these figures exhibits a large out-of-phase

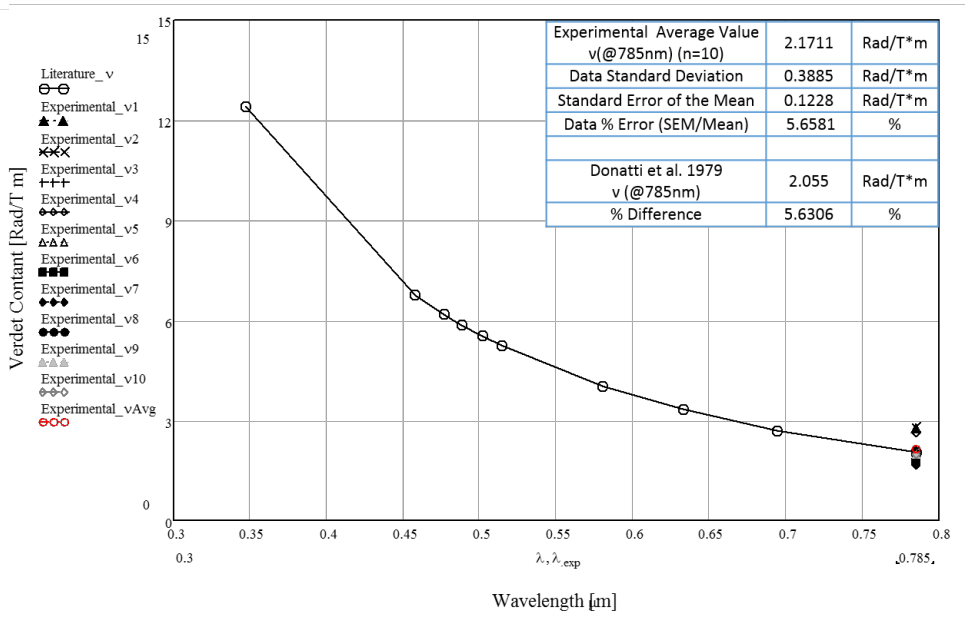


**Figure 4.2:** Comparison of experimental verdet constant (Black Triangle) at 785 nm with literature values reported by Villaverde et al. [36]

component, although the field was measured directly using a gaussmeter probe. This is due to electronic phase lag and not to the sample properties (negligible response in this case for an empty core). This lag was expected to be seen in all experiments due to the nature of the invariant field response. All studies focused on applying this phase lag correction to the experiments for samples of varying materials to determine the true out-of-phase response.

### 4.2.2 Frequency Domain AC Sample Characterization: Initial Results

#### NBK7 Standard Sample: Magneto-Optical Phase Lag Correction Response Confirmation

The first step in determining the accuracy of this system was the confirmation of the phase lag correction for a standard sample (3.0 mm window of NBK7 glass). A similar signal response is observed from Fig. 4.5 to Fig. 4.6 as was seen for the magnetic field measurements in the last section. Interestingly, the phase correction starts to fail as the

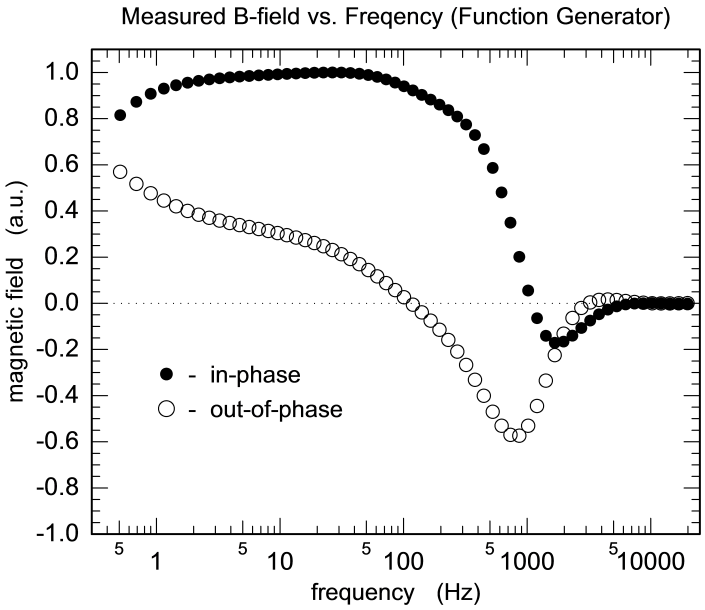


**Figure 4.3:** Magnetic field measurement with significant phase lag across frequency spectrum

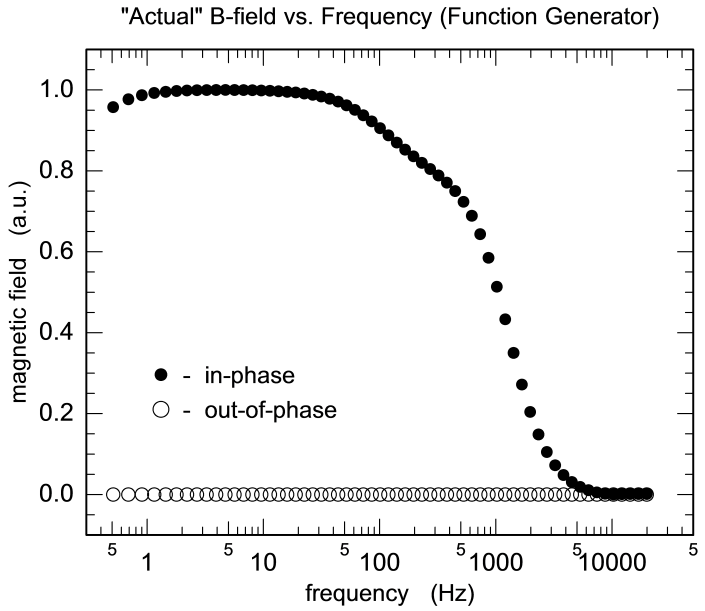


**Figure 4.4:** Adjusted magnetic field measurement with phase lag adjusted across frequency spectrum

frequency increases beyond approximately 200 Hz, likely due to the lack of exactitude of the interpolating function used for the phase correction program or the change in current source

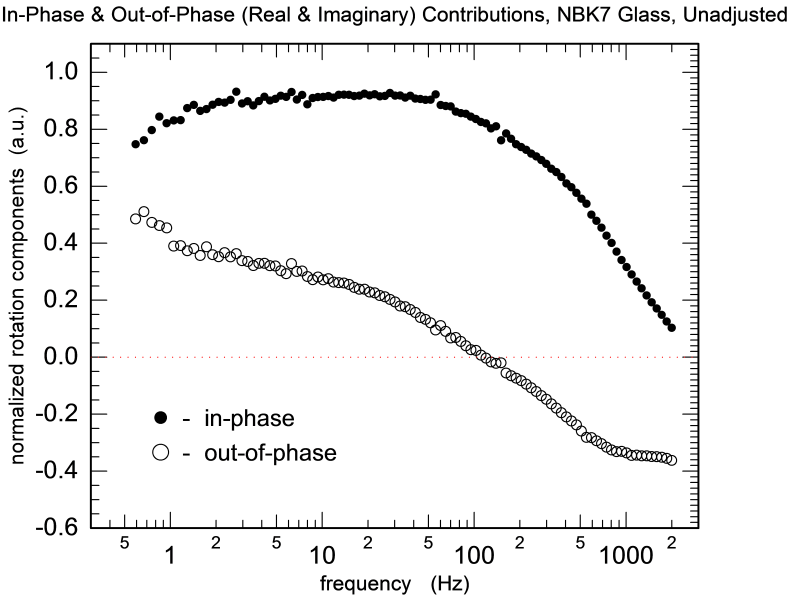


**Figure 4.5:** Example of unadjusted data for NBK7 glass sample

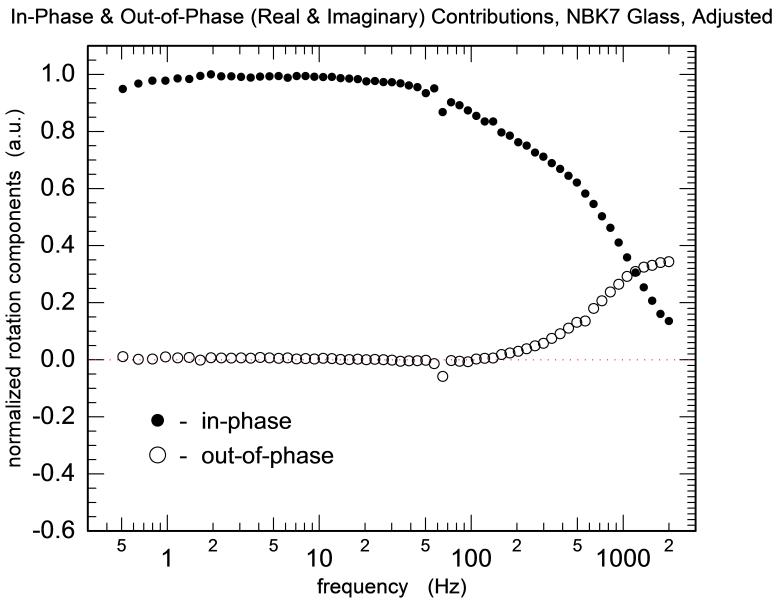


**Figure 4.6:** Example of phase adjusted data for NBK7 glass sample with imperfect phase lag correction

channel on the Linear Amplifier from experimental adjustments.

### DDW, 1$\mu$m Streptavadin Coated Dynabeads, and 200 to 500 nm Magnetic Nanoparticles: Normalized Phase Adjusted Data

Of the experiments that were run to test the fd-FRS system, the most representative results were obtained from phase adjusted TGG (crystal standard with a very large verdet constant, on the order of 80 $\frac{Rad}{T*m}$), DDW and nanoparticle samples in Fig. 4.7 with an example calibration used in Fig. 4.8. The initial data indicate that the responses for dilute particle suspensions is incredibly similar to that for the pure water sample. A significant 60 Hz broad electronic noise peak is seen to obscure the data and prevent the individual particle rotation peaks to be seen. This is not the spread of spectra to be used for final verdet constant comparison with literature as the noise floor is large, but they do show how close this project currently is to obtaining the proper spectra for materials characterization. It is also noteworthy that the normalization of this data set was with respect to the largest response in the set, in this case for the Dynabeads at 0.01 V%. Future work will also address the differences in calibration curve responses due the differing laser powers on the photodetector due to sample scattering and absorbance. The expected response of this system is included in red as shown in this figure. The ideal scenario would be no 60 Hz noise, a large and sharp peak corresponding to the brownian relaxation out-of-phase response, and a near-zero out-of-phase response elsewhere.

### Verdet Constant Determination: Normalized Phase Adjusted Data

Comparison of the data presented in Fig. 4.7 and Fig. 4.9, it can be seen that dividing the in and out-of-phase responses for experimental data by the coresponding magnetic field at each frequency then normalizing yields a plot of comparable verdet constant plots. This data can be compared across materials (note that normalization removes the magnitude of the verdet constant, allowing only for peak location analysis). When 60 Hz noise is cancelled,

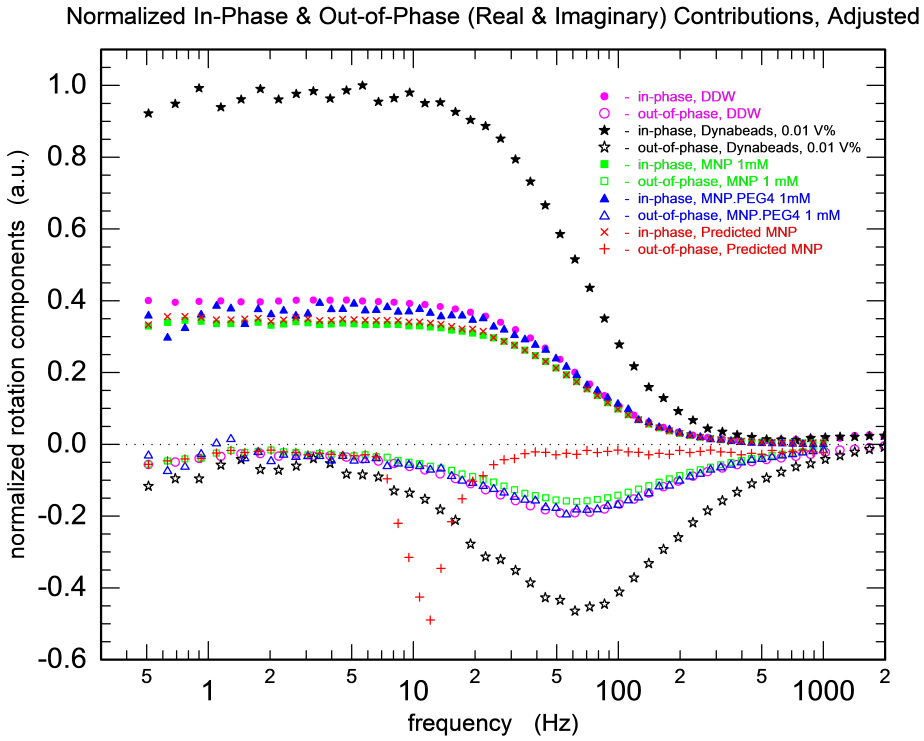


**Figure 4.7:** Faraday rotation responses of 4 example material systems for the location and determination of peaks in maximum response (Dynabeads) normalized representation. An expected response spectra is also included for comparison

this data is expected to show the clearest peaks, even clearer than expected for the faraday rotation response. This is due to the inclusion of the consideration of field strength at each frequency point, thus allowing for accurate comparison across any frequency domain magnetic field.

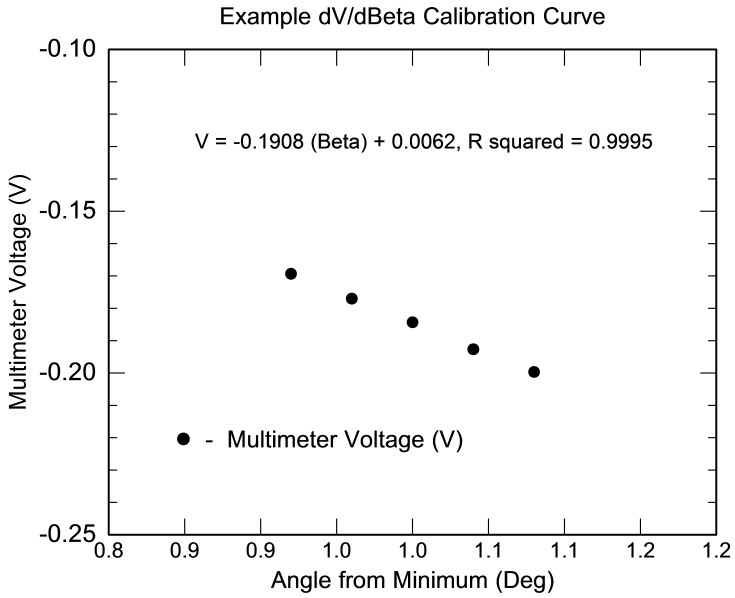


**Figure 4.8:** Example calibration curve obtained from clean NBK7 glass window sample

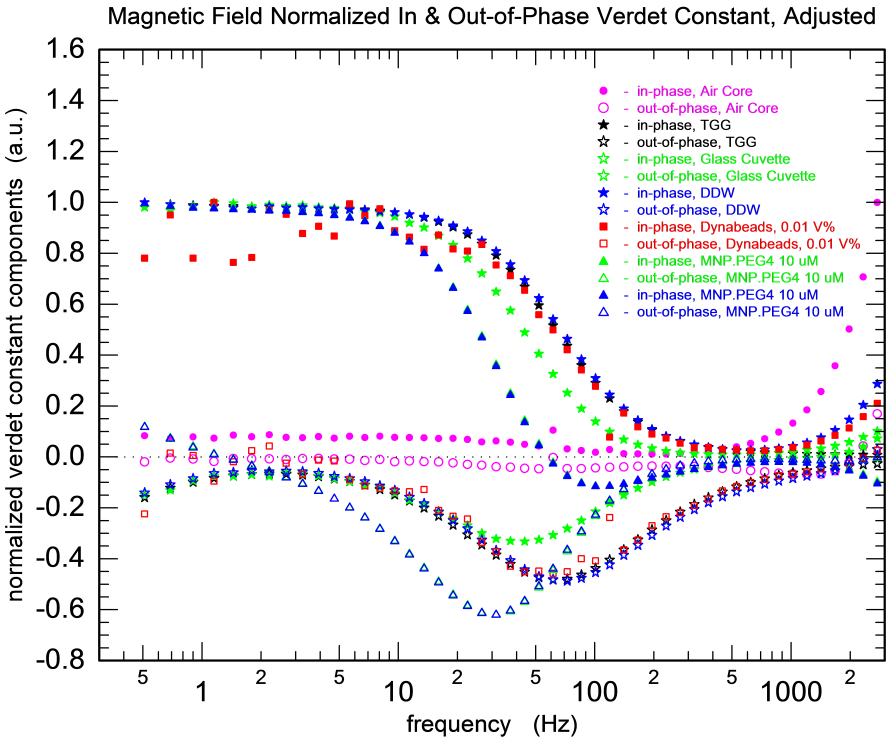


**Figure 4.9:** Experimental results for normalized $\nu$ real and imaginary components derived from the components in Eq. 3.8 - 3.9 and adjusted by Eq. 3.17 - 3.18. Note the presence of 60 Hz noise and the deviation of the in-phase response from the ideal magnetic field response in Fig. 4.4

# CHAPTER 5: CONCLUSIONS

Frequency Domain Faraday Rotation Spectroscopy (fd-FRS) has shown potential to complement current immunoassay and materials characterization methods. Phase adjustment and noise reduction have eliminated background noise and allowed for comparisons among solid, pure liquid, and colloidal suspension samples, yet at this point in the work, clear peaks are not observed where they should be. It was observed that agglomeration/sedimentation of the ferrofluids, overall polydispersity, and optical noise level do not allow for clear peaks to be seen in the data so far. In order to prevent sedimentation, the ideal particle concentration and size range for best signal-to-noise ratio can be determined. Samples ranging from Terbium Gallium Garnet crystal and borosilicate glass to magnetic particles ranging from 200 nm to 1 $\mu$m in size exhibited responses corresponding to the applied field with enough accuracy to measure their verdet constants. The 60 Hz noise observed to date as well as the need for a reduced noise floor and monodisperse particle samples (for sharp peaks) limits the current utility of the fd-FRS technique. Such is the nature of this project as the development of the spectroscopy method must be refined further to bring this technique to the forefront of scientific research in magneto-optical techniques and clinical application. It is seen that this work has completed its initial objectives to (1) study the frequency-dependence of the faraday rotation in ferrofluids and (2) to extend this system to elucidating particle size and conformation as an alternative immunoassay to costly and labor/time intensive Western Blotting and ELISA, although the results are preliminary. Results will be compared to ELISA and Western Blotting techniques for sensitivity and highly monodisperse particle samples will be tested to detect clean and sharp peaks.

The development of a technique to study the surface functionalization of multi-functional beads/nanoparticles will open the door to even greater sensitivity and control in the devel-

opment of nanoscale biomedical technologies. Much as NMR revolutionized the characterization scene upon its development, novel methods of spectroscopy could potentially provide opportunities to conduct new biomedical research at the nanoscale. With the successful completion of this project, extensions of this work could see developments in characterization of complex, multi-component particles with multiple functional layers of material or characterization of multiple biomolecules at once. The shapes and sizes of the nanoprobes could be varied to determine the effect of spatial variation of biomolecule faraday rotation on the surface of slowly rotating particles. Stronger fields, on the order of several Tesla could be developed to ensure even the weakest of diamagnetic biomolecules would be accurately probed by this technique. Due to the diamagnetic nature of all materials, fd-FRS could be improved to extend the response expected to be observed with iron oxide nanoparticles/beads to nanoprobes made of polymers, non-superparamagnetic metallic compounds such as gold nanoparticles, or purely organic/biological systems. One could also couple magneto-optical responses to thermal behavior in surface protein conformation and materials characterization (metal-insulator transitions). Lastly, although the proposed project outlines only the magnetic frequency-domain response of the systems under study, theoretically the electromagnetic radiation absorption in the near and far IR could be coupled to the current experiments in a pump-probe technique to determine complex vibrational, rotational, as well as electronic modes of biomolecule motion at the surface of magnetic particles.

# BIBLIOGRAPHY


[1] A. P. Astalan, F. Ahrentorp, C. Johansson, K. Larsson, and A. Krozer. Biomolecular reactions studied using changes in brownian rotation dynamics of magnetic particles. *Biosensors and Bioelectronics*, 19(8):945–951, 2004.

[2] K. Aurich, G. Glöckl, S. Nagel, and W. Weitschies. Magneto-optical relaxation measurements of functionalized nanoparticles as a novel biosensor. *Sensors*, 9(6):4022–4033, 2009.

[3] K. Aurich, G. Glöckl, E. Romanus, P. Weber, S. Nagel, and W. Weitschies. Magneto-optical relaxation measurements for the characterization of biomolecular interactions. *Journal of Physics: Condensed Matter*, 18(38):S2847, 2006.

[4] K. Aurich, S. Nagel, G. Glöckl, and W. Weitschies. Determination of the magneto-optical relaxation of magnetic nanoparticles as a homogeneous immunoassay. *Analytical chemistry*, 79(2):580–586, 2007.

[5] K. Aurich, S. Nagel, E. Heister, and W. Weitschies. Affinity analysis for biomolecular interactions based on magneto-optical relaxation measurements. *Nanotechnology*, 19(50):505102, 2008.

[6] N. P. Barnes and L. B. Petway. Variation of the verdet constant with temperature of terbium gallium garnet. *JOSA B*, 9(10):1912–1915, 1992.

[7] W. Brullot, N. K. Reddy, J. Wouters, V. K. Valev, B. Goderis, J. Vermant, and T. Verbiest. Versatile ferrofluids based on polyethylene glycol coated iron oxide nanoparticles. *Journal of Magnetism and Magnetic Materials*, 324(11):1919–1925, 2012.

[8] Y. Chemla, H. Grossman, Y. Poon, R. McDermott, R. Stevens, M. Alper, and J. Clarke. Ultrasensitive magnetic biosensor for homogeneous immunoassay. *Proceedings of the National Academy of Sciences*, 97(26):14268–14272, 2000.

[9] X. Chen, B. Lavorel, J. Boquillon, R. Saint-Loup, and M. Jannin. Optical rotary power at the resonance of the terbium 7f6→ 5d4 line in terbium gallium garnet. *Solid-State Electronics*, 42(9):1765–1766, 1998.

[10] X. Chi, D. Huang, Z. Zhao, Z. Zhou, Z. Yin, and J. Gao. Nanoprobes for¡ i¿ in vitro¡/i¿ diagnostics of cancer and infectious diseases. *Biomaterials*, 33(1):189–206, 2012.

[11] S.-H. Chung, M. Grimsditch, A. Hoffmann, S. D. Bader, J. Xie, S. Peng, and S. Sun. Magneto-optic measurement of brownian relaxation of magnetic nanoparticles. *Journal of Magnetism and Magnetic Materials*, 320(3):91–95, 2008.

[12] R. J. Falconer and A. G. Markelz. Terahertz spectroscopic analysis of peptides and proteins. *Journal of Infrared, Millimeter, and Terahertz Waves*, 33(10):973–988, 2012.

[13] G. Glöckl, V. Brinkmeier, K. Aurich, E. Romanus, P. Weber, and W. Weitschies. Development of a liquid phase immunoassay by time-dependent measurements of the transient magneto-optical birefringence using functionalized magnetic nanoparticles. *Journal of magnetism and magnetic materials*, 289:480–483, 2005.

[14] S. P. Gubin. *Magnetic nanoparticles*. John Wiley & Sons, 2009.

[15] D. Jacob, M. Vallet, F. Bretenaker, A. Le Floch, and R. Le Naour. Small faraday rotation measurement with a fabry–perot cavity. *Applied physics letters*, 66(26):3546–3548, 1995.

[16] L. Kalandadze. Faraday rotation and magneto-optical figure of merit for the magnetite magnetic fluids. In *EPJ Web of Conferences*, volume 15, page 01028. EDP Sciences, 2011.

[17] A. Kaminskii, H. Eichler, P. Reiche, and R. Uecker. Srs risk potential in faraday rotator tb3ga5o12 crystals for high-peak power lasers. *Laser Physics Letters*, 2(10):489–492, 2005.

[18] D. Klein. *Organic Chemistry*. Wiley, 2011.

[19] O. Koo, A. Aroonnual, and A. Bhunia. Human heat-shock protein 60 receptor-coated paramagnetic beads show improved capture of listeria monocytogenes in the presence of other listeria in food. *Journal of applied microbiology*, 111(1):93–104, 2011.

[20] R. Kötitz, W. Weitschies, L. Trahms, W. Brewer, and W. Semmler. Determination of the binding reaction between avidin and biotin by relaxation measurements of magnetic nanoparticles. *Journal of magnetism and magnetic materials*, 194(1):62–68, 1999.

[21] B. Y. Ku, M.-L. Chan, Z. Ma, and D. A. Horsley. Frequency-domain birefringence measurement of biological binding to magnetic nanoparticles. *Journal of magnetism and magnetic materials*, 320(18):2279–2283, 2008.

[22] B. T. Kurien and R. H. Scofield. Western blotting. *Methods*, 38(4):283–293, 2006.

[23] J. Lange, R. Kötitz, A. Haller, L. Trahms, W. Semmler, and W. Weitschies. Magnetorelaxometry—a new binding specific detection method based on magnetic nanoparticles. *Journal of magnetism and magnetic materials*, 252:381–383, 2002.

[24] M. Maiorov. Faraday effect in magnetic fluids at a frequency 10ghz. *Journal of magnetism and magnetic materials*, 252:111–113, 2002.

[25] J.-M. Montenegro, V. Grazu, A. Sukhanova, S. Agarwal, M. Jesus, I. Nabiev, A. Greiner, and W. J. Parak. Controlled antibody/(bio-) conjugation of inorganic nanoparticles for targeted delivery. *Advanced drug delivery reviews*, 65(5):677–688, 2013.

[26] D. Pagliero, Y. Li, S. Fisher, and C. Meriles. Approach to high-frequency, cavity-enhanced faraday rotation in fluids. *Applied optics*, 50(5):648–654, 2011.

[27] Y. Pan, C. Du, X. Liu, Z. Li, and R. Birngruber. Wavelength dependence of the faraday effect and magnetobirefringence in ferrofluid thin films. *Journal of applied physics*, 73(10):6139–6141, 1993.

[28] C. Pang, C. Hsieh, and J. Lue. A study of magneto-optical effect in dilute fe3o4 ferrofluid by attenuated total reflection, ferromagnetic resonance and faraday rotation. *Journal of Physics D: Applied Physics*, 36(15):1764, 2003.

[29] C. W. Pratt, D. Voet, and J. G. Voet. Fundamentals of biochemistry: life at the molecular level, 2013.

[30] S. Puertas, P. Batalla, M. Moros, E. Polo, P. del Pino, J. M. Guisan, V. Grazu, and J. M. de la Fuente. Taking advantage of unspecific interactions to produce highly active magnetic nanoparticle- antibody conjugates. *ACS nano*, 5(6):4521–4528, 2011.

[31] F. Royer, D. Jamon, J. J. Rousseau, V. Cabuil, D. Zins, H. Roux, and C. Bovier. Experimental investigation on $\gamma$- fe2o3 nanoparticles faraday rotation: particles size dependence. *The European Physical Journal Applied Physics*, 22(02):83–87, 2003.

[32] N. T. Thanh. *Magnetic Nanoparticles: From Fabrication to Clinical Applications*. CRC Press, 2012.

[33] N. V. Tkachenko. *Optical spectroscopy: methods and instrumentations*. Elsevier, 2006.

[34] K. Turvey. Determination of verdet constant from combined ac and dc measurements. *Review of scientific instruments*, 64(6):1561–1568, 1993.

[35] V. Vasyliev, P. Molina, M. Nakamura, E. G. Víllora, and K. Shimamura. Magneto-optical properties of tb 0.81 ca 0.19 f 2.81 and tb 0.76 sr 0.24 f 2.76 single crystals. *Optical Materials*, 33(11):1710–1714, 2011.

[36] A. B. Villaverde and D. Donatti. Verdet constant of liquids; measurements with a pulsed magnetic field. *The Journal of Chemical Physics*, 71(10):4021–4024, 1979.

[37] A. B. Villaverde, D. Donatti, and D. Bozinis. Terbium gallium garnet verdet constant measurements with pulsed magnetic field. *Journal of Physics C: Solid State Physics*, 11(12):L495, 1978.

[38] S. Wang, C. Sun, L. Du, C. Yao, and Y. Yang. Reciprocity of faraday effect in ferrofluid: Comparison with magneto-optical glass. *Optik-International Journal for Light and Electron Optics*, 123(6):553–558, 2012.

[39] S. Woodford, A. Bringer, and S. Bluegel. Interpreting magnetization from faraday rotation in birefringent magnetic media. *Journal of Applied Physics*, 101(5):053912, 2007.

[40] D. Worcester. Structural origins of diamagnetic anisotropy in proteins. *Proceedings of the National Academy of Sciences*, 75(11):5475–5477, 1978.

[41] X. Zhang, D. B. Reeves, I. M. Perreard, W. C. Kett, K. E. Griswold, B. Gimi, and J. B. Weaver. Molecular sensing with magnetic nanoparticles using magnetic spectroscopy of nanoparticle brownian motion. *Biosensors and Bioelectronics*, 50:441–446, 2013.